To cite this version :

A. BOUDIS, A. C. BAYEUL-LAINÉ, A. BENZAOUI, H. OUALLI, O. GUERRI, O. COUTIER-DELGOSHA - Numerical Investigation of the Effects of Nonsinusoidal Motion Trajectory on the Propulsion Mechanisms of a Flapping Airfoil - Journal of Fluids Engineering - Vol. 141, n°4, p.041106 - 2019

A. Boudis

LTSE,
Faculty of Physics,
University of Science and Technology
Houari Boumediene (USTHB),
BP 32 El-Alia,
Algiers 16111, Algeria
e-mail: aboudis@usthb.dz

A. C. Bayeul-Lainé

LMFL,
Arts et Métiers ParisTech,
8 Boulevard Louis XIV,
Lille 59046, France

A. Benzaoui

LTSE,
Faculty of Physics,
University of Science and Technology
Houari Boumediene (USTHB),
BP 32 El-Alia,
Algiers 16111, Algeria

H. Oualli

LMF,
Ecole Militaire Polytechnique,
BP 17 Bordj-el-Bahri,
Algiers 16046, Algeria

O. Guerri

Centre de Développement des
EnergiesRenouvelables, CDER,
BP 62, Route de l'Observatoire,
Bouzareah,
Algiers 16340, Algeria

O. Coutier-Delgosha

Virginia Tech,
Kevin T. Crofton Department of
Aerospace and Ocean Engineering,
Blacksburg, VA 24061

Numerical Investigation of the Effects of Nonsinusoidal Motion Trajectory on the Propulsion Mechanisms of a Flapping Airfoil

The effect of nonsinusoidal trajectory on the propulsive performances and the vortex shedding process behind a flapping airfoil is investigated in this study. A movement of a rigid NACA0012 airfoil undergoing a combined heaving and pitching motions at low Reynolds number (Re = 11,000) is considered. An elliptic function with an adjustable parameter S (flattening parameter) is used to realize various nonsinusoidal trajectories of both motions. The two-dimensional (2D) unsteady and incompressible Navier–Stokes equation governing the flow over the flapping airfoil are resolved using the commercial software STAR CCM+. It is shown that the nonsinusoidal flapping motion has a major effect on the propulsive performances of the flapping airfoil. Although the maximum propulsive efficiency is always achievable with sinusoidal trajectories, nonsinusoidal trajectories are found to considerably improve performance: a 110% increase of the thrust force was obtained in the best studied case. This improvement is mainly related to the modification of the heaving motion, more specifically the increase of the heaving speed at maximum pitching angle of the foil. The analysis of the flow vorticity and wake structure also enables to explain the drop of the propulsive efficiency for nonsinusoidal trajectories.

1 Introduction

In aeronautics, the field of micro-air vehicle (MAV), and in particular micro-air vehicle with flapping wing, is one of the most studied subjects in recent years. The remarkable interest in the study of these small aircraft is linked to the advantages of this locomotion mode. Unlike the fixed-wing, flapping-wing MAVs are able to perform hovering or low-speed flight in the manner of insects or humming birds with very high maneuverability. To perform punctual tasks, the flapping wings offer the advantage related to the acoustic spectrum generally lower than that created by the rotating wings. In addition, flapping wing MAVs develop a higher lift force than those of the fixed and rotating wings due to nonstationary flow aspects. To generate the same lift force, the latter need more energy supply.

Historically, Knoller [1] and Betz [2] are among the pioneers to suggest a quasi-steady approach to explain the lift and thrust generation mechanism using a flapping wing. The Knoller-Betz effect stipulates that during a flapping motion, wings create an unsteady effective angle of attack due to the transversal velocity, generating consequently an aerodynamic force with both lift and thrust components. In 1922, Katzmayr [3] carried out the first experimental work to verify the Knoller-Betz effect and to confirm the possibility of thrust production using flapping wings. Thereafter, von Karman and Burgers [4] provide the relationship between the wake nature and the drag or thrust production. A drag-indicative wake (Fig. 1(*a*)), similar to the von Karman eddy street observed behind a bluff body, is formed when the lower vortex row is counterclockwise and the upper clockwise. The reverse von Karman vortex street (Fig. 1(*b*)) with clockwise upper vortex and counterclockwise lower vortex is a thrust-indicative wake. A year later, Theodorsen [6] successfully calculated the unsteady forces and moments generated by an airfoil in harmonic motion using the hypothesis of incompressible potential flow with the Kutta condition at the trailing edge. Subsequently, Garrick [7] continued the work of Theodorsen [6] where he theoretically showed that an
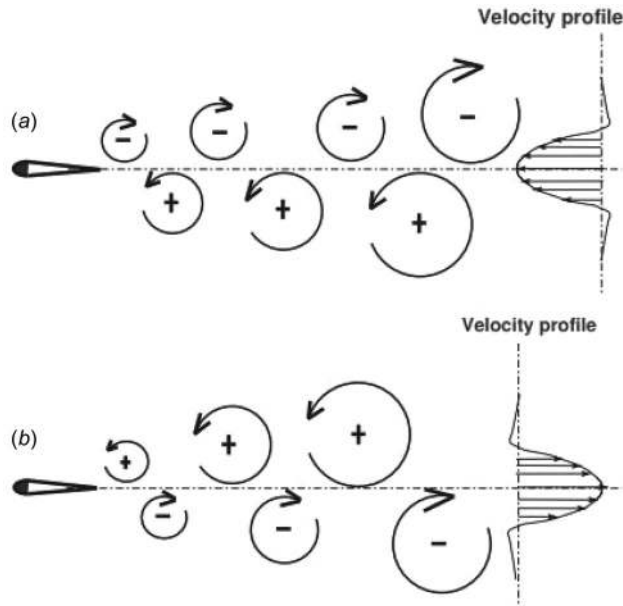
Fig. 1   Vortical patterns in the wake of a flapping airfoil [5]: (*a*) drag-indicative wake and (*b*) thrust-indicative wake

airfoil in pure heaving motion generates thrust for all frequencies, while a pure pitching airfoil generates thrust above a certain critical frequency.

Since the first works of thrust generation from flapping airfoil, several experimental [8–15] and numerical [16–23] studies were carried out to understand the mechanism of thrust generation and to improve their propulsive performances. A large number of these works focused on the effect of kinematic parameters such as the maximum amplitudes of heaving and pitching motions, the phase angle between heaving and pitching motions, the flapping frequency, and the effective angle of attack on the propulsive performance of the flapping airfoil. The published results indicated that the best propulsive performances were obtained when the Strouhal number was in the range of (0.2–0.4), the angle of attack was set between 20 deg and 30 deg, and the phase angle was in the range (80–100 deg).

Other works dealt with the influence of the geometric parameters such as the airfoil thickness, camber, and flexibility. Among these studies, Ashraf et al. [24] investigated numerically the effect of thickness and camber on the propulsive performances of a flapping airfoil at different flow regimes, laminar and turbulent. They showed that at low Reynolds number, the thin profile had better performances compared to the thick profile. They also showed that the profile camber did not affect the propulsive performances. Deng and Xiao [25] carried out numerical investigations to study the effect of chordwise flexion on the propulsive performances of flapping wings in terms of thrust generation, power consumption, and propulsive efficiency. Their results showed that the chordwise flexibility had a positive role on the enhancement of the propulsive performances.

Previously, it was shown that the use of nonsinusoidal flapping trajectory could improve the propulsive performances. Koochesfahani [26] and Read et al. [27] observed, experimentally, that the use of nonsinusoidal flapping trajectory improved the thrust generation. Hover et al. [28] experimentally investigated the effect of the angle of attack profile on the propulsive performance of a harmonically heaving and pitching foil. Four trajectory types are considered: harmonic motion, a square wave, a symmetric sawtooth wave, and a cosine function. Their results showed that the cosine angle of attack achieves a significant improvement over the other three cases, in the sense of high thrust values with reasonable efficiency. Their results showed also that the sawtooth profile

improves the thrust coefficient by 12.12% when compared to the cosine profile at high Strouhal number (St = 0.8). Sarkar and Venkatraman [29] investigated the effect of nonsinusoidal motion on the propulsive performance of an airfoil executing a heaving motion. Three motion modes are considered: asymmetric, sinusoidal, and constant heave rate oscillations motions. The conclusion was that asymmetric motion leads to better thrust and propulsive efficiency in comparison to sinusoidal motion. However, constant rate heave motion does not favorably compare with sinusoidal heaving motion. Kaya and Tuncer [30] conducted a two-dimensional (2D) numerical study to investigate the effect of the nonsinusoidal trajectory on the propulsive performances of a flapping airfoil. The nonsinusoidal trajectory was realized by a third-degree nonuniform rational B-splines function (NURBS). They found that an optimized nonsinusoidal flapping trajectory improved significantly the thrust force compared to the sinusoidal flapping motion. Kaya and Tuncer [31] used the same nonsinusoidal trajectory (NURBS) as in Kaya and Tuncer [30] to optimize the propulsive performances of dual airfoils in a biplane configuration. A significant improvement was also obtained. Xiao and Liao [32] performed a numerical study to investigate the effect of asymmetric sinusoidal trajectory on the propulsion performances of a pitching NACA0012 airfoil. Their results showed that the higher asymmetry motion induced the stronger reverse von Karman vortex street. Thus, the thrust force was increased. Xiao and Liao [33] conducted a numerical study devoted to the effect of effective angle of attack profile on the propulsion performance of a NACA0012 foil undergoing heaving and pitching motion with an effective angle of attack evolving as a harmonic cosine function. To this aim, either the heaving or pitching motion was modified from a sinusoidal form. The results showed that a cosine profile of the effective angle of attack improved considerably the propulsive performance. In addition, better performance was obtained when the modification was imposed on the pitching motion. Lu et al. [34] numerically considered the effects of the amplitude, camber and nonsinusoidal motion on the aerodynamic characteristics of a pitching airfoil operating in propulsive mode. They found that better thrust force was always generated with largest pitching amplitudes. At low amplitudes, the thrust force increased rapidly with increasing the pitching amplitude up to a threshold angle and then the increase in thrust force was slowed. On the other hand, the propulsive efficiency decreased significantly with the increase of the pitching amplitude at a fixed reduced frequency. They noticed also that the camber has a negligible effect on the thrust generation and that the use of a nonsinusoidal pitching motion improved substantially the thrust production. They also reported the major effect of nonsinusoidal motion on the flow structures and development of vortices. Esfahani et al. [35] numerically studied the effect of the elliptical motion trajectory on the aerodynamic characteristics and propulsive performances of a flapping airfoil. The elliptical motion was achieved by combination of a horizontal motion (forward/backward) with a vertical motion (heaving). They pointed out that elliptical motion trajectories change both the effective angle of attack and the vortex shedding pattern. Therefore, they significantly influence the aerodynamic and propulsive performances of the flapping airfoil. Yang et al. [36] carried out a numerical simulation dealing with the influence of the motion trajectory on the aerodynamic performances of an airfoil undergoing three combined motions: a rotating motion (pitch), a horizontal motion (surge), and a vertical motion (plunge). It is reported that the figure-of-eight motion trajectory improves the thrust, lift, and propulsive efficiency of the flapping airfoil. They have also shown that multiple vortices generation contributes to enhance the instantaneous force over the flapping airfoil.

The purpose of the present work is to study the effect of motion trajectory on the propulsive performances and the vortex shedding mechanism of a flapping airfoil. For that purpose, the commercial code STAR CCM+ is used to solve the unsteady and incompressible Navier–Stokes equations that govern the flow over the airfoil. The
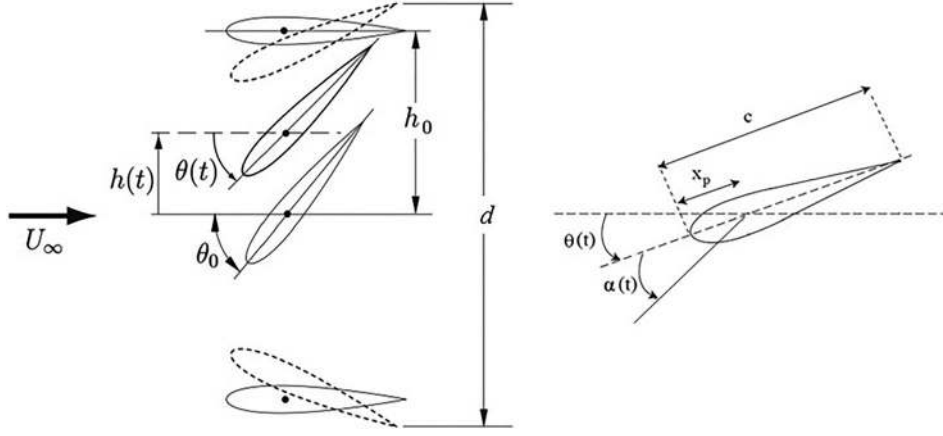
Fig. 2 Main kinematic parameters of a flapping airfoil (Adapted from Ref. [37])

imposed flapping motions are reproduced using the overset mesh technique available in the environment of this software. Reliability and accuracy of the numerical procedure are examined by comparing the computed results with experimental and numerical literature results [9,19]. Then the effect of nonsinusoidal motions is presented in Sec. 3 and the mechanisms responsible for the changes in the propulsive force and efficiency are discussed in Sec. 4.

2 Numerical Modelization

2.1 Flapping Motion Kinematics. The sinusoidal flapping motion of an airfoil (Fig. 2) is given by the following equations:

$$h(t) = h_0 c \cos(\omega t) \tag{1}$$

$$\theta(t) = \theta_0 \cos(\omega t + \phi) \tag{2}$$

where $h(t)$ and $\theta(t)$ are the heaving and the pitching motions, respectively, h_0 is the heaving amplitude, θ_0 is the pitching amplitude, $\omega = 2\pi f$ is the angular frequency, c is the chord length, and ϕ is the angle phase between the heaving and the pitching motions. The pitch axis is located at 1/3 of the chord from leading edge.

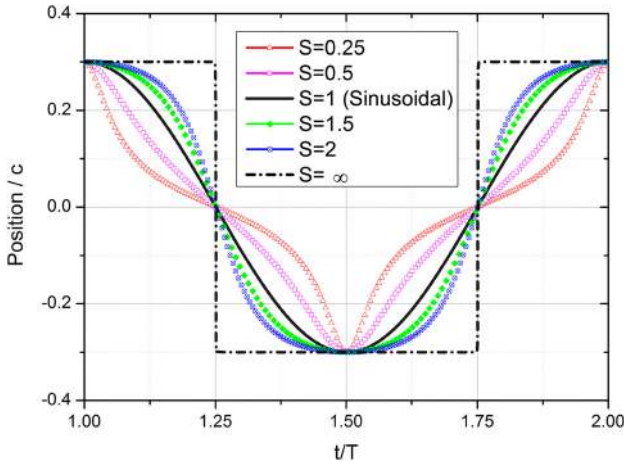The nonsinusoidal flapping motion is realized using an elliptical trajectory defined by the following equation:

Fig. 3 Flapping trajectories according to different values of the flattening parameter S

$$F(t) = \frac{S \cos(\omega t)}{\sqrt{S^2 \cos(\omega t)^2 + \sin(\omega t)^2}} \tag{3}$$

where S is a flattening parameter. As shown in Fig. 3, when $S = 1$, the elliptical trajectory is sinusoidal. If S tends to infinity a square trajectory is obtained.

In the case of a nonsinusoidal trajectory, the combined heaving and pitching motions can be represented by

$$h_0(t) = h_0 c \frac{S_h \cos(\omega t)}{\sqrt{S_h^2 \cos(\omega t)^2 + \sin(\omega t)^2}} \tag{4}$$

$$\theta(t) = \theta_0 \frac{S_\theta \cos(\omega t + \phi)}{\sqrt{S_\theta^2 \cos(\omega t + \phi)^2 + \sin(\omega t + \phi)^2}} \tag{5}$$

where S_h and S_θ are the flattening parameters of heaving and pitching trajectory, respectively.

When the airfoil is moving, the effective angle of attack $\alpha(t)$ is the sum of the pitching angle and the induced angle due to heaving motion. Thus, the angle is given by the relation

$$\alpha(t) = \arctan\left(\frac{1}{U_\infty} \frac{dh(t)}{dt}\right) - \theta(t) \tag{6}$$

In addition, two dimensionless parameters are used to characterize the propulsive performance of the flapping airfoil. The Strouhal number defined by Anderson et al. [9] as $\mathrm{St} = 2cfh_0/U_\infty$ and the Reynolds number based on the chord length of the airfoil, $\mathrm{Re} = \rho c U_\infty/\mu$, where ρ is the flow density, U_∞ is the freestream velocity, and μ is the dynamic viscosity.

2.2 Thrust and Propulsive Efficiency Definition. The propulsive performance of a flapping airfoil can be quantified by calculating the mean thrust coefficient $\bar{C}_t$, the mean power coefficient $\bar{C}_p$, and the propulsive efficiency η

$$\bar{C}_t = -\frac{1}{T} \int_0^T C_D(t) dt \tag{7}$$

$$\bar{C}_p = -\frac{1}{T} \int_0^T \left(\frac{1}{U_\infty} C_L(t) \frac{dh(t)}{dt} + \frac{c}{U_\infty} C_Z(t) \frac{d\theta(t)}{dt} \right) dt \tag{8}$$

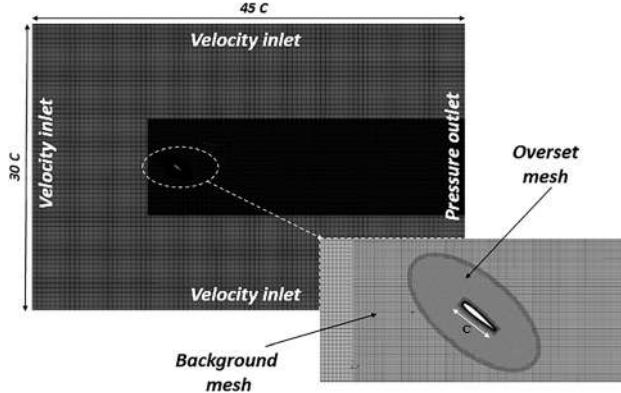$$\eta = \frac{\bar{C}_t}{\bar{C}_p} \tag{9}$$

Fig. 4 Computational domain and boundary conditions

where T is the period of motion. C_D, C_L, and C_Z are, respectively, the drag, lift and moment coefficients, defined as follows:

$$C_D = \frac{F_x}{0.5\rho A U_\infty^2}, \quad C_L = \frac{F_y}{0.5\rho A U_\infty^2}, \quad C_Z = \frac{M_z}{0.5\rho c A U_\infty^2} \quad (10)$$

where $A = 1c$ is the area of the airfoil.

The pitching axis is located at 1/3 of the chord length from the leading edge.

2.3 Fluid Equations. The fluid flow around the flapping airfoil is governed by the unsteady incompressible Navier–Stokes equations, which can be written in 2D and nondimensional form as follows:

$$\frac{\partial u}{\partial t} = -u\frac{\partial u}{\partial x} - v\frac{\partial u}{\partial y} - \frac{1}{\rho}\frac{\partial p}{\partial x} + \nu\left(\frac{\partial^2 u}{\partial x^2} + \frac{\partial^2 v}{\partial y^2}\right) \quad (11)$$

$$\frac{\partial v}{\partial t} = -u\frac{\partial v}{\partial x} - v\frac{\partial v}{\partial y} - \frac{1}{\rho}\frac{\partial p}{\partial y} + \nu\left(\frac{\partial^2 u}{\partial x^2} + \frac{\partial^2 v}{\partial y^2}\right) \quad (12)$$
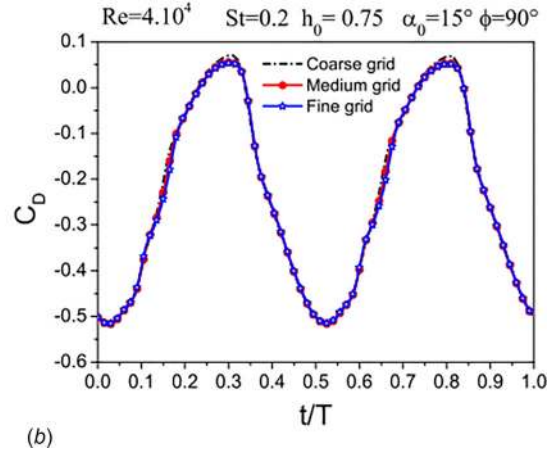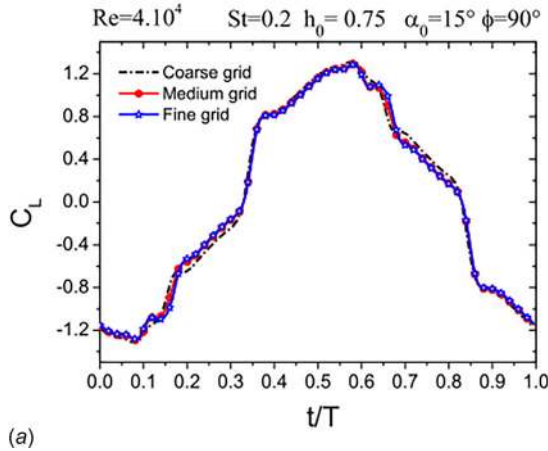
The continuity equation is given by the following form:

$$\frac{\partial u}{\partial x} + \frac{\partial v}{\partial y} = 0 \quad (13)$$

where t is the time, u and v are velocity components, p is the pressure, ρ is the fluid density, and ν is the kinematic viscosity.

2.4 Solver. The unsteady flow field around the flapping airfoil was simulated using the finite volume code STAR-CCM+. A segregated pressure-based solver was used to solve the Navier–Stokes equations with a pressure–velocity coupling achieved by the semi-implicit method for pressure-linked equations. Second-order schemes are used for the pressure and momentum discretization and the unsteady formulation is based on a second-order implicit scheme. All simulations are carried out at a Reynolds number, Re = 11,000. Therefore, the flow regime is considered laminar and incompressible (more details about the solver can be found in STAR-CCM+ user guide [38]). The numerical results are assumed converged when the variation of the propulsive efficiency between two successive periods does not exceed 1%. Then, the calculations are continued for five flapping cycles to ensure that periodic solution is achieved.

2.5 Computational Domain and Boundaries Conditions. The foil considered in the present work is the NACA0012 symmetrical profile. The dimensions of the computational domain and the boundary conditions used in this study are schematically shown in Fig. 4. At inlet, top, and bottom boundaries, the pressure is set to zero gradient and the fluid velocity in x direction is specified based on the desired Reynolds number. At outlet, the pressure is equal to freestream pressure and the outlet velocity is set to

Fig. 5 Grid independence study

Table 1 Grid and time-step independence study

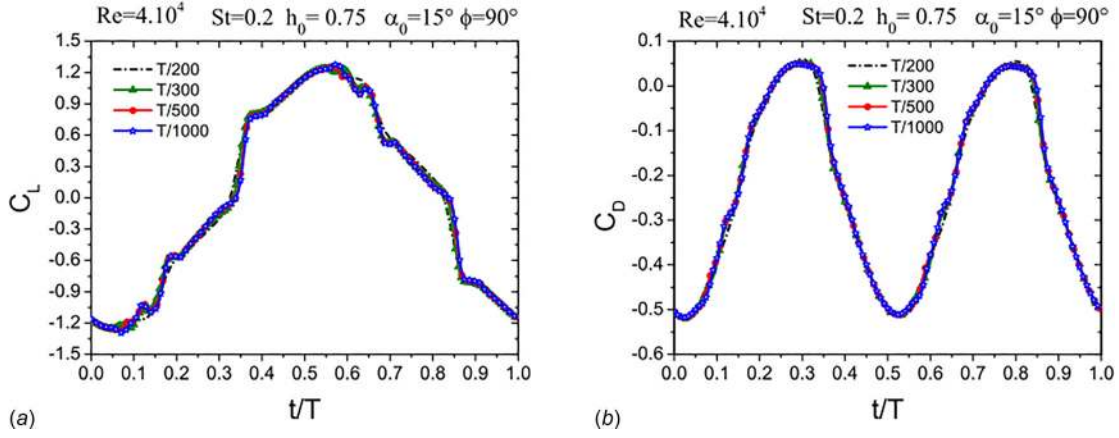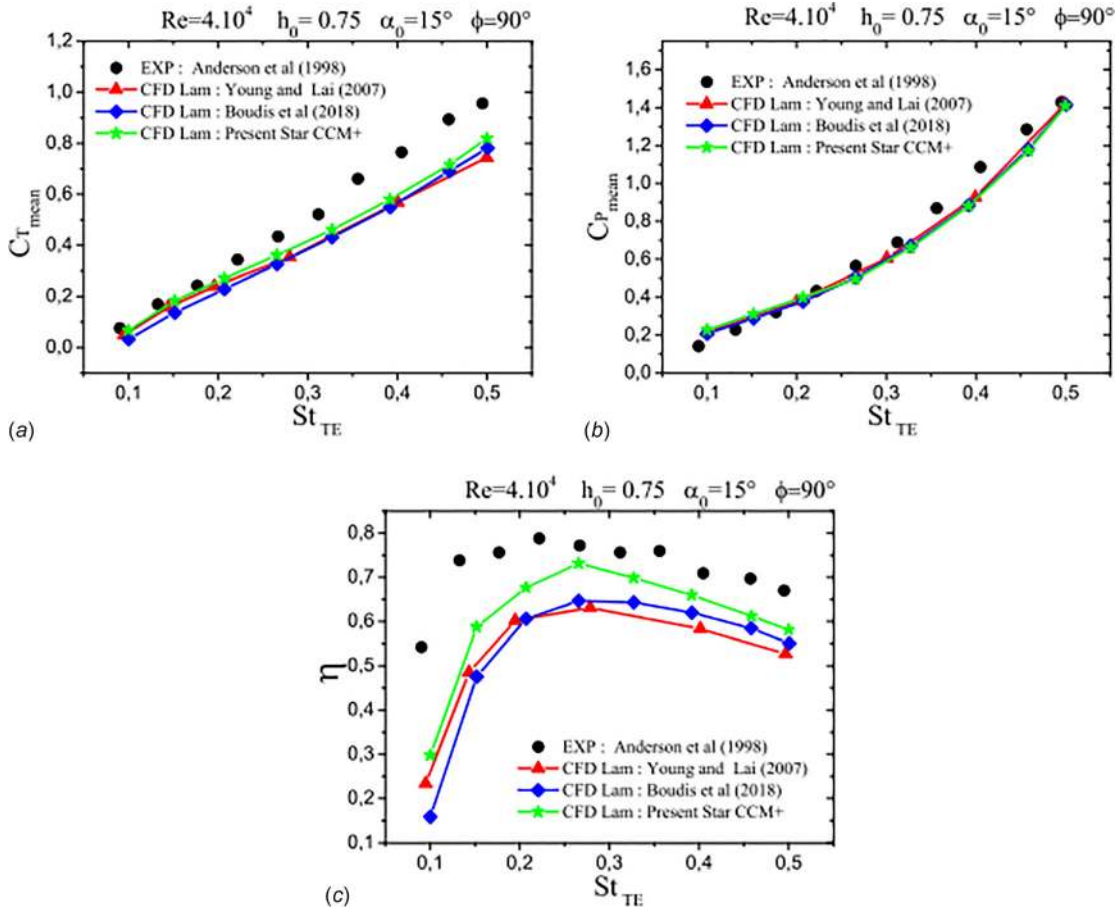|	Mesh	Time-step	$\bar{C}_D$	Mean error	$\bar{C}_L$	Mean error
Grid independence	Coarse grid	$T/200$	−0.22939	1.875%	0.24058	0.312%
	Medium grid		−0.23422	0.213%	0.24011	0.116%
	Fine grid		−0.23372	—	0.23983	—
Time-step independence	Medium grid	$T/200$	−0.23422	3.203%	0.24011	2.157%
		$T/300$	−0.23027	1.462%	0.23822	1.352%
		$T/500$	−0.22722	0.118%	0.2367	0.706%
		$T/1000$	−0.22695	—	0.23504	—

Fig. 6   Time-step independence study

Fig. 7   Variation of $\bar{C}_t$, $\bar{C}_p$, and η with St_{TE}

zero gradient. On the airfoil surface, the no-slip condition is imposed. The domain is subdivided into two zones: a background zone and an overset zone. The airfoil is located in the zone 1 (overset zone). This zone is moving to ensure the heaving and pitching motions. It is meshed with a very fine structured mesh to accurately capture the gradients in the area close to the airfoil surface. As in Ref. [20], the first grid point is located at $10^{-5}c$ giving y^+ less than 1. The second zone (background) is also meshed with a structured mesh but less dense compared with the first zone to decrease the cells number and improve the calculation efficiency. The connection between the two zones is ensured using the overset mesh interface [38]. The overset mesh technique allows to simulate the combined heaving and pitching motions without using other techniques such as deforming mesh or remeshing.

2.6   Grid and Time Step Independence Study. A sensitivity study is performed to determine the grid refinement and time-step required to ensure that the results do not depend on these numerical settings. These simulations are performed with the following parameters: Re = 40,000, St = 0.2, $h_0 = 0.75$, $\phi = 90$ deg, and $\alpha_0 = 15$ deg. First, the study is carried out using three grids with different mesh density. The total number of cells is 47,760 for the coarse grid, 87,760 for the medium grid, and 254,400 for the fine

Table 2   Cases analyzed

	Flattering coefficient S	
	S_h	S_θ
Reference case	1	1
Case 1	0.25 0.5 1.5 2	1
Case 2	1	0.25 0.5 1 2
Case 3	0.25 0.5 1 2	0.25 0.5 1 2

grid. The time-step is set to $\Delta t = T/200$ in all cases. Figure 5 shows the temporal variation of the lift and drag coefficients over one flapping cycle obtained with the three grids. It is shown that the difference between the results obtained with the medium grid and the fine grid is negligible. Indeed, the difference between the mean C_D and C_L coefficients is 0.213% and 0.116%, respectively (see Table 1). Therefore, the medium grid is considered sufficiently fine to obtain reliable results. Next, the independence study of the time-step size on the computed results is performed using four different time-steps: $T/200$, $T/300$, $T/500$, and $T/1000$. The medium grid is applied for these simulations. Figure 6

displays the time variation of the lift and drag coefficients over one flapping cycle computed with the different time steps. This figure shows that the results obtained with $\Delta t = T/500$ are close to those obtained with $\Delta t = T/1000$. The difference between the mean C_D and C_L coefficients is 0.118% and 0.706%, respectively (see Table 1). Thus, the time-step $\Delta t = T/500$ and the medium grid are used in the following simulations.

2.7 Validation. To confirm the accuracy of the present approach, the computed results were compared with some experimental data available in the literature, for the same foil geometry and a Reynolds number $Re = 40,000$. The propulsive performance generated by a combined heaving and pitching motions is calculated using the following kinematic parameters $h_0 = 0.75$, $\alpha_0 = 15$ deg, and $\phi = 90$ deg and a Strouhal number St_{TE} varying in the range of (0–0.5), ($St_{TE} = fd/U_\infty$, where d is the maximum excursion of the trailing edge [9]). In Fig. 7, the thrust coefficient, the power coefficient, and the propulsive efficiency obtained in the present simulation are compared to the experimental data reported in Ref. [9]. Other numerical results obtained previously in the same flow configuration by Young and Lai [19] and the present authors with the code FLUENT [39] are also reported. All numerical results, including the present ones, are in fair agreement with the experiments: for a Strouhal number lower than 0.3, the thrust and the power coefficients are especially close to the experimental data, while they are significantly underestimated in all simulations at higher values of St_{TE}. However, the thrust obtained in the present work compares slightly better with the experiments than the previous simulations, in all cases, which results in a propulsive efficiency in much better agreement with the measurements. These results generally confirm that the present simulation is able to capture the important features of the flow generated by the flapping foil.
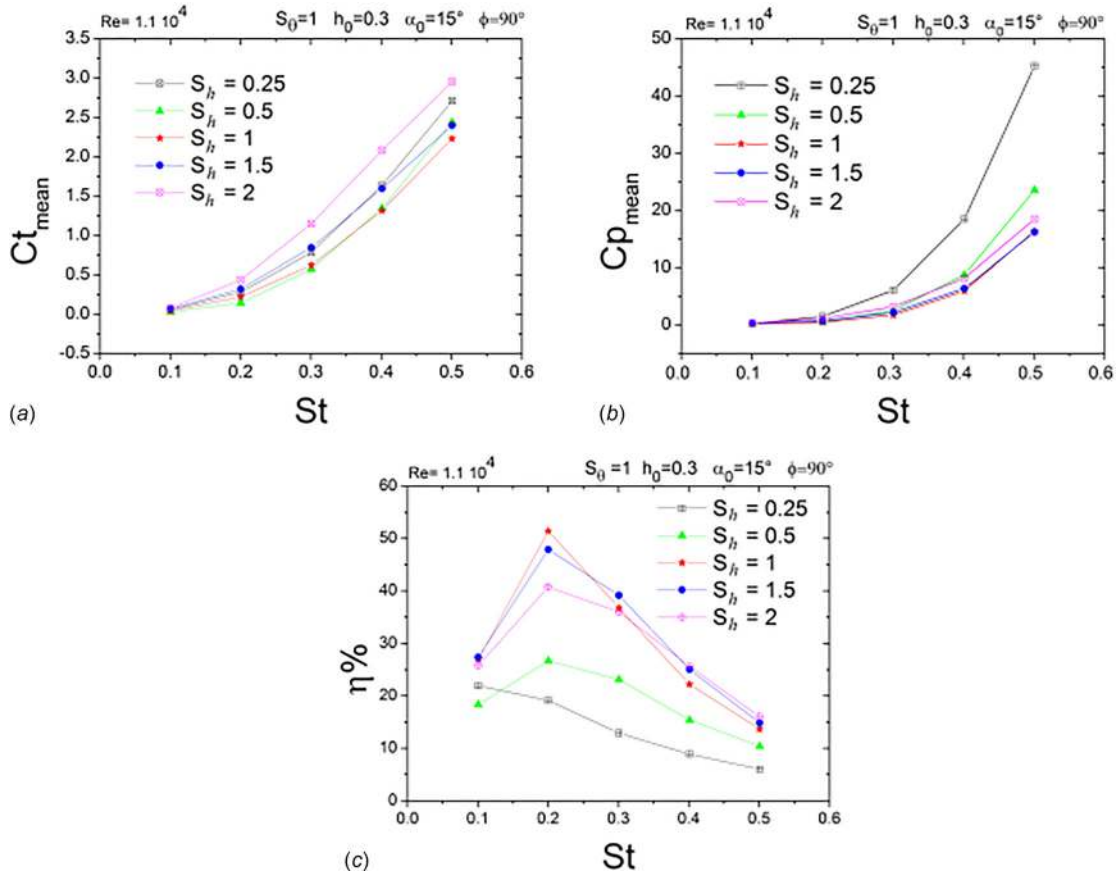

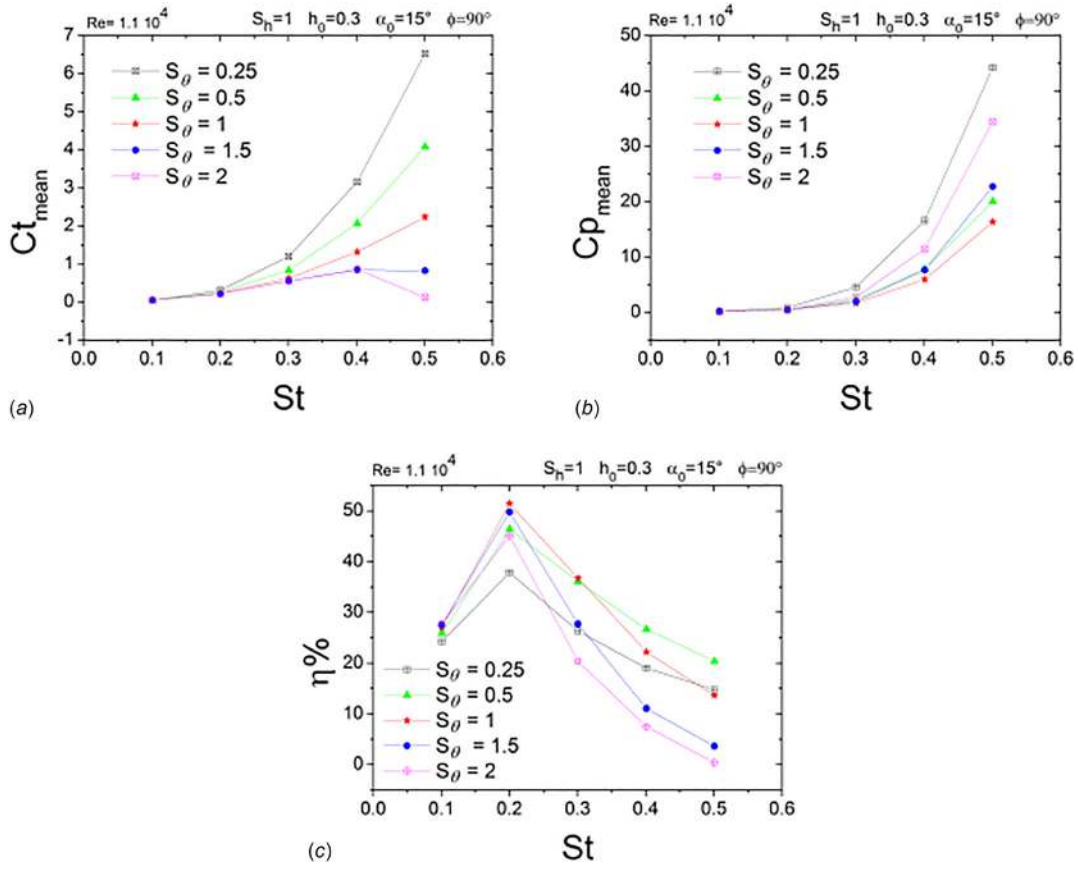Fig. 8   Effect of nonsinusoidal heaving, case 1
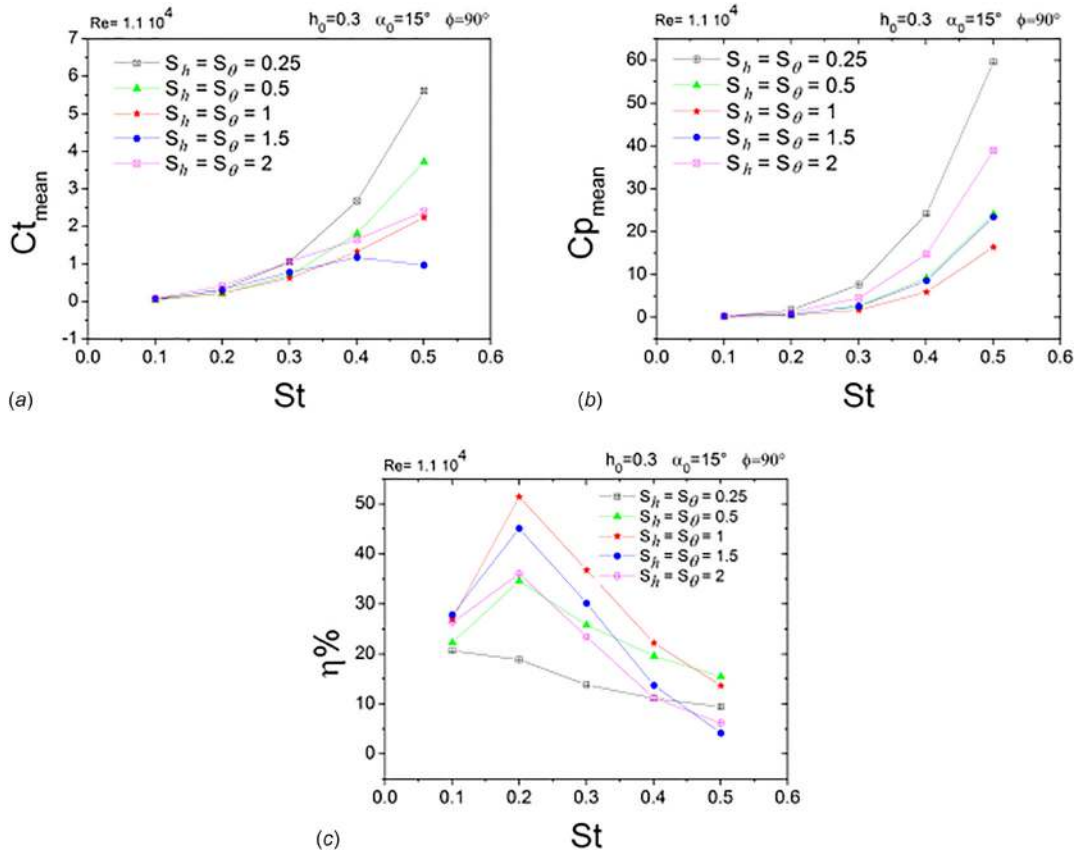
Fig. 9   Effect of nonsinusoidal pitching, case 2

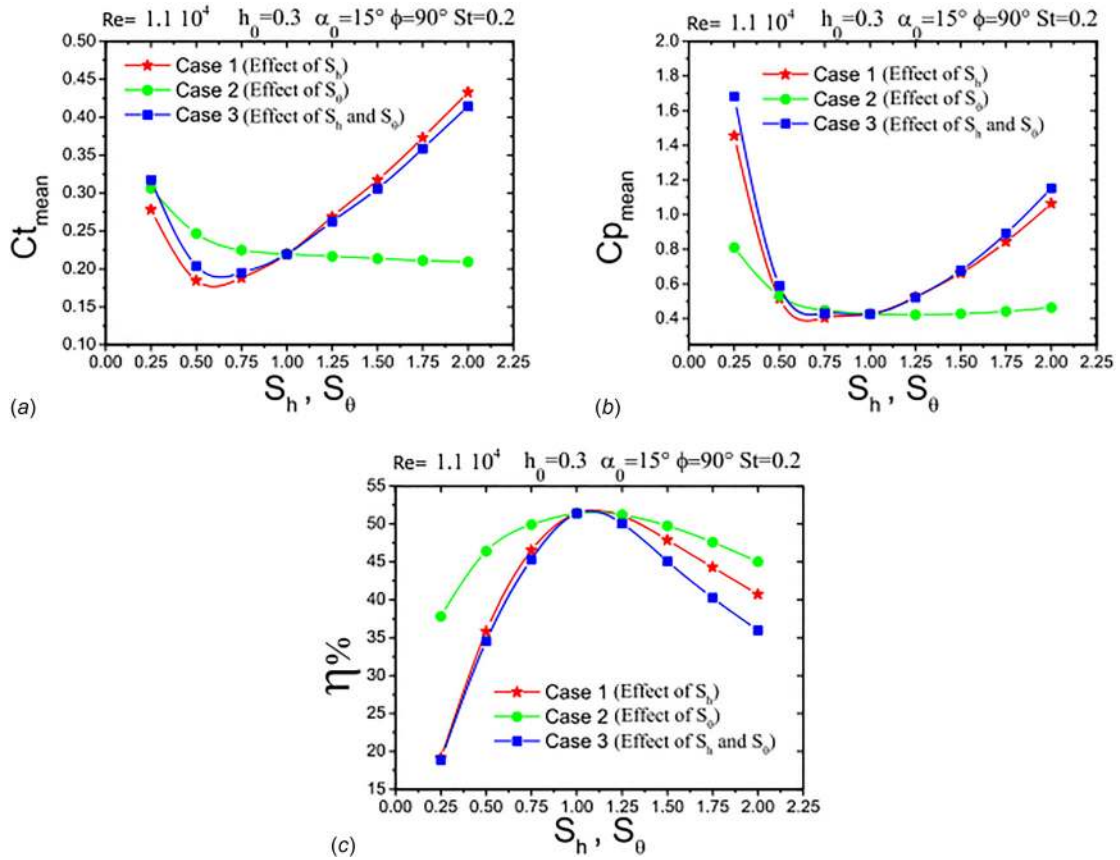Fig. 10   Effect of nonsinusoidal heaving and pitching motions, case 3

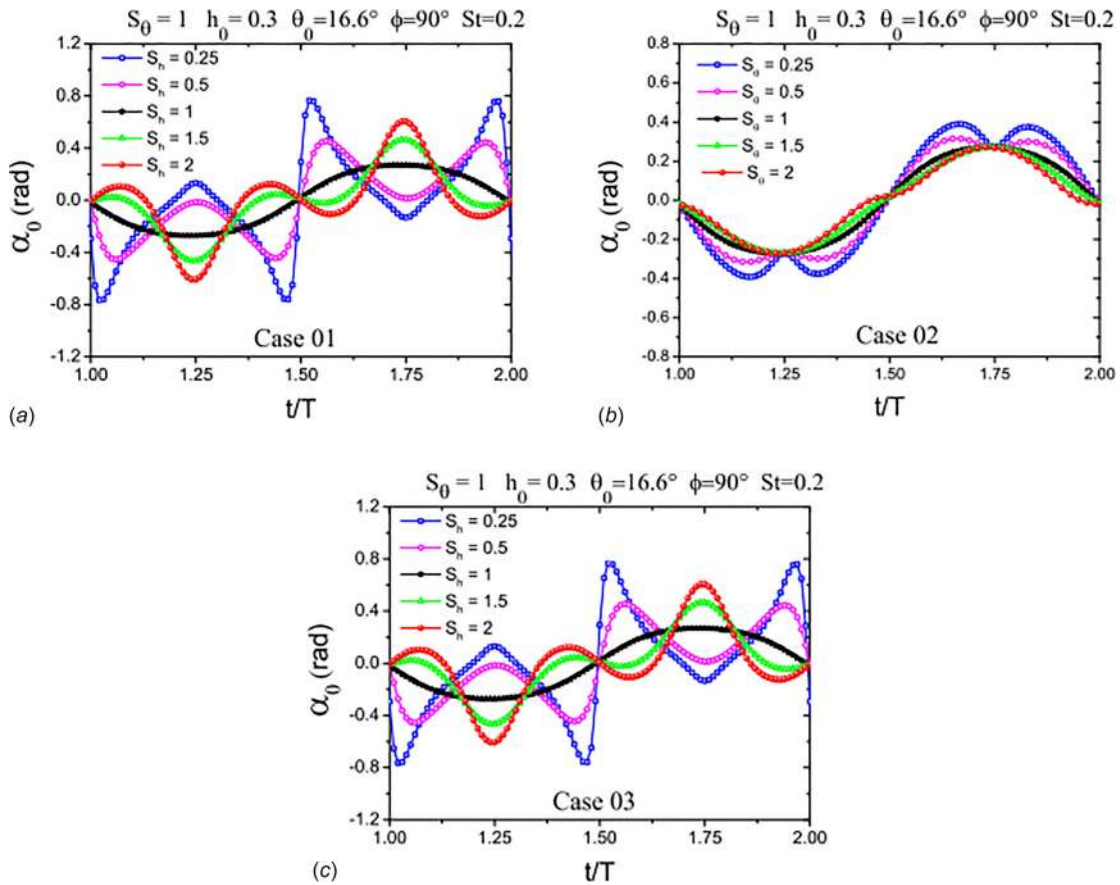**Fig. 11 Effect of the flapping trajectory on the propulsion performances**

Fig. 12 Effect of the flapping trajectory on the kinematic angle of attack
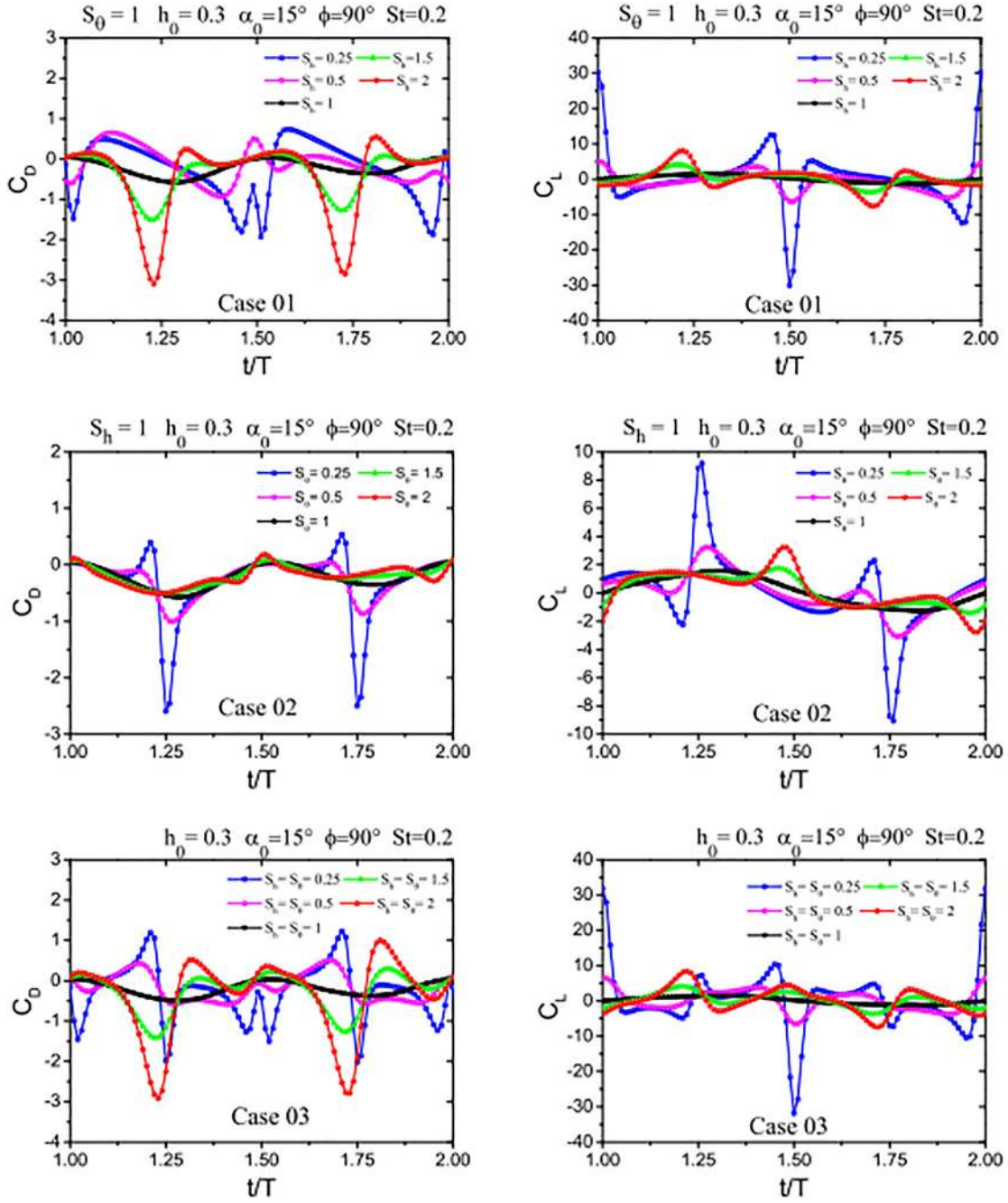
Fig. 13 Time variation of C_D and C_L under the effect of nonsinusoidal motion

3 Results

The main objective of the present study is to evaluate and analyze the effects of nonsinusoidal flapping trajectory on the propulsive performance and on the vortex formation, shedding process, and the wake pattern behind a flapping airfoil. Indeed, the wake structure downstream from the trailing edge is strongly related to the forces generated by a flapping airfoil and its propulsive performance [33]. To carry out this study, three cases are considered:

Case 1: Nonsinusoidal heaving combined with sinusoidal pitching motions.
Case 2: Sinusoidal heaving combined with nonsinusoidal pitching motions.
Case 3: Nonsinusoidal heaving and pitching motions.

To study the effect of motion trajectory, the kinetics parameters are fixed as: $h_0 = 0.3$, $\phi = 90\,\text{deg}$, $\alpha_0 = 15\,\text{deg}$, $St \in [0.1 - 0.5]$,

and Re = 11,000. The nonsinusoidal trajectory is obtained by modifying the flattening parameter in the range of (0.25–2). The obtained results are compared to those of a sinusoidal trajectory case to show the influence of the nature of motion trajectory on the airfoil propulsive performance. Table 2 summarizes the studied cases.

3.1 Effect of Strouhal Number. In this section, the effect of Strouhal number St on the performance of the flapping airfoil is investigated. The variation of the mean thrust coefficient ($\bar{C}_t$), mean power coefficient ($\bar{C}_p$), and the propulsive efficiency η with St for different values of S_h and S_θ are shown in (Figs. 8–10). In case 1, it is observed that the increase in the Strouhal number induces an increase of the mean thrust coefficient and the mean power coefficient. This is in good agreement with the experimental results of Ref. [9]. These authors mentioned that the mean
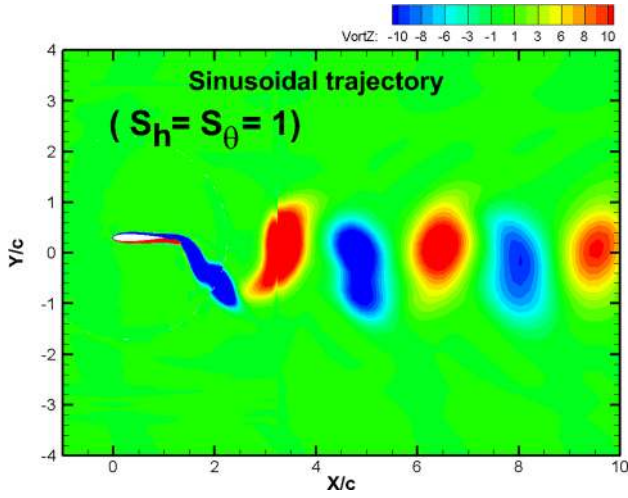
Fig. 14 The 2S vortex shedding mode

coefficient of thrust increases continuously with the increase of the Strouhal number. In case 2, it is observed that at high Strouhal numbers (greater than 4), the use of flattening parameters greater than 1.5 causes a decrease in the mean thrust coefficients and dramatically augmentation in the mean power coefficients. Same remark was observed in case 3 for the flattening parameter ($S_h = S_\theta = 1$). It is also observed that the propulsive efficiency increases with the increase of the Strouhal number up to a threshold value St = 0.2 and then decreases. This decreasing tendency is due to the fact that, at high Strouhal numbers, the power consumed increases rapidly to maintain the flapping motion.

3.2 Effect of Nonsinusoidal Trajectory. The effect of nonsinusoidal trajectory on the propulsive performances of a flapping airfoil is investigated for a fixed Strouhal number (St = 0.2, corresponding to best propulsive efficiency). The obtained results are presented in Fig. 11. It is seen that the propulsive efficiency obtained with sinusoidal trajectory is always better than that obtained by the nonsinusoidal trajectory regardless the value of the flattening parameter. On the other hand, the thrust force obtained with nonsinusoidal trajectories is notably improved relatively to the sinusoidal trajectories. A simple comparison reveals that the nonsinusoidal heaving motion leads to a better improvement than that on the nonsinusoidal pitching motion. For a nonsinusoidal heaving, the largest propulsive force is obtained for trajectories corresponding to flattening parameter values larger than 1. Conversely, for nonsinusoidal pitching, the best propulsive force is obtained with the trajectories realized with flattening parameters less than 1 ($S_\theta < 1$). In this situation, the power consumed to maintain the flapping motion is weak comparatively to the other cases. This results in a better propulsive efficiency whatever is the value of the flattening parameter. For all the considered situations, it is found that using trajectories with the flattening parameters lower than 0.5 requires more energy to maintain the flapping motion. Moreover, the heaving trajectory is found to have a larger effect on propulsive performances of the flapping airfoil compared to the pitching trajectory. This is mainly due to the change in the effective angle of attack profile induced by the nonsinusoidal heaving motion.

Figure 12 shows the time variation of the effective angle of attack for the considered three cases during one flapping cycle. According to this figure, the nonsinusoidal flapping motion has a great effect on the effective angle of attack profile, which confirms that it is an essential parameter that directly impacts the propulsive performance of a flapping airfoil [28].
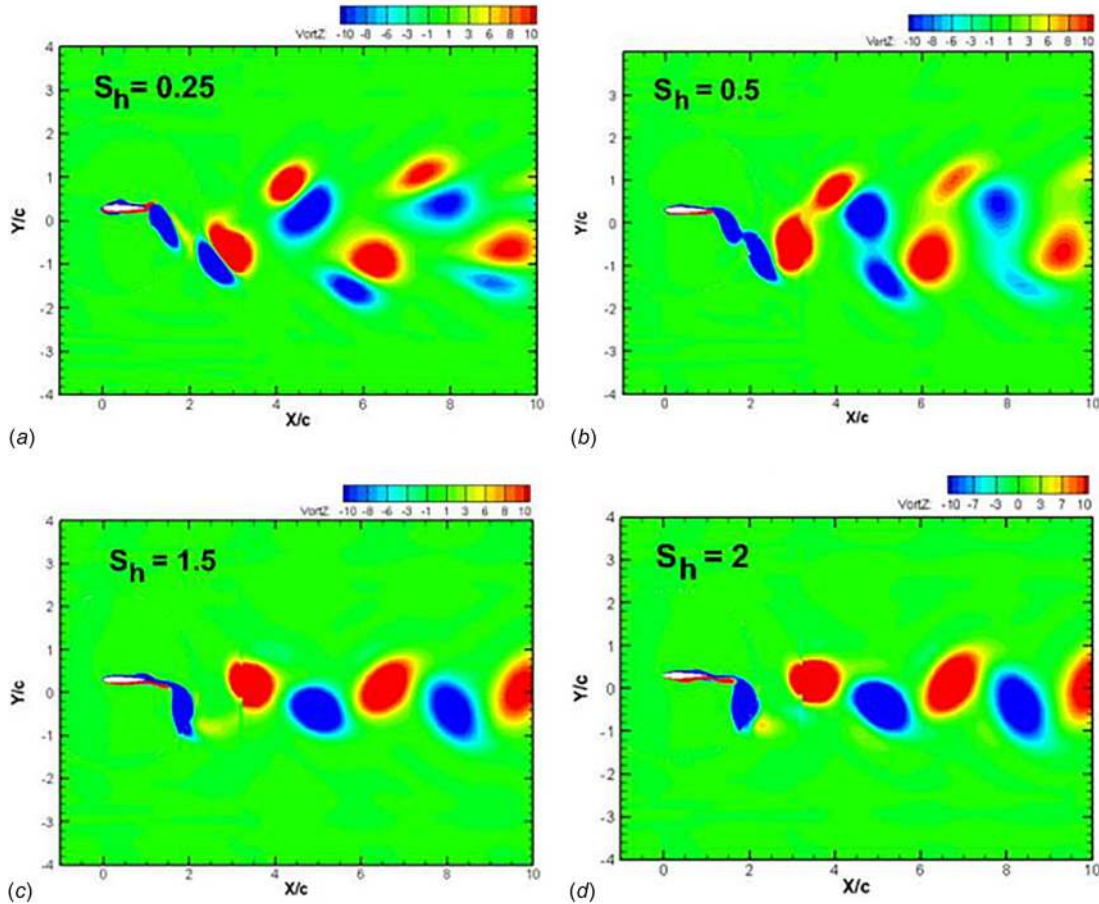

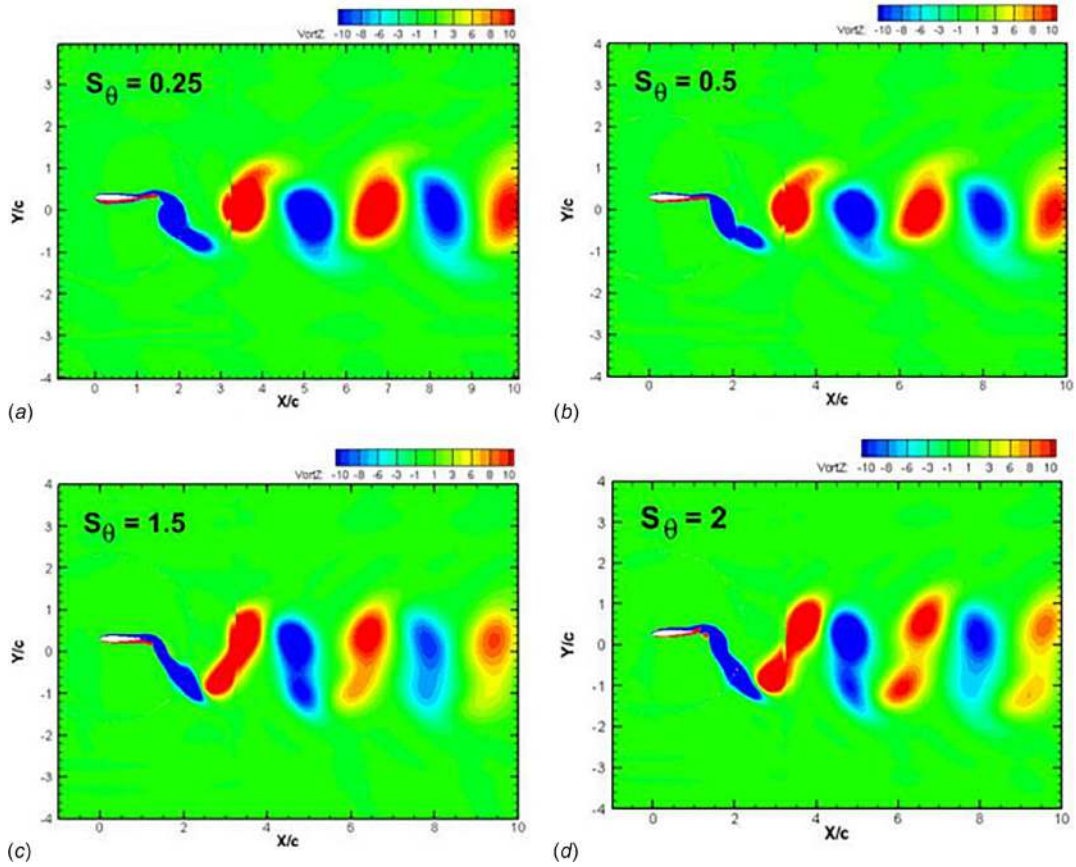**Fig. 15 Modes of vortex shedding and the wake pattern, case 1**

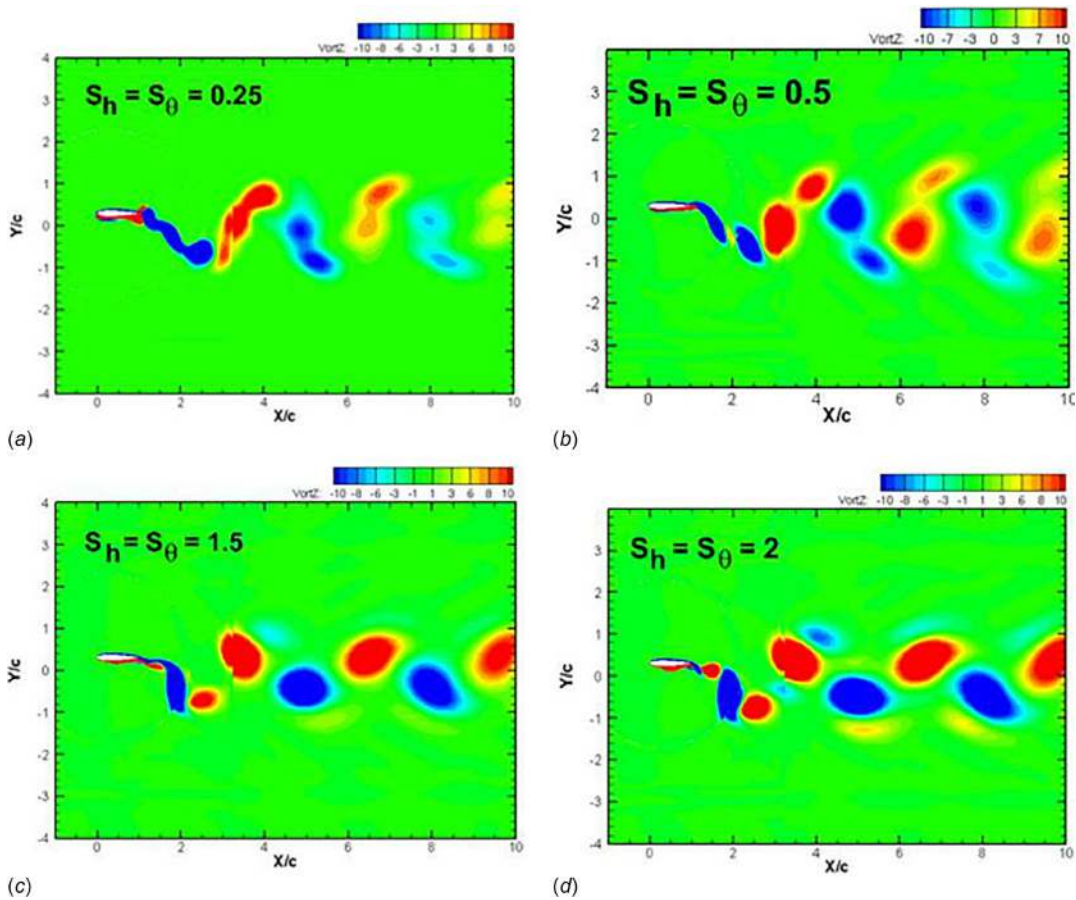**Fig. 16 Modes of vortex shedding and the wake pattern, case 2**

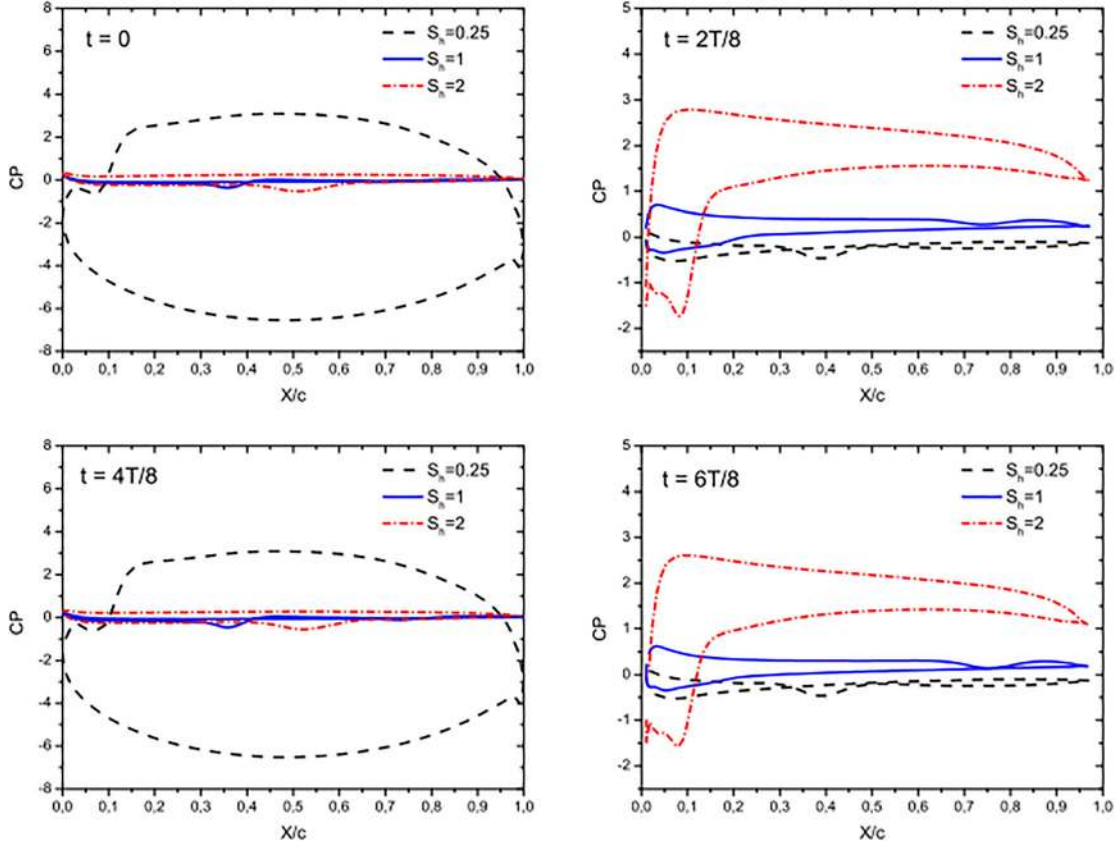
Fig. 17 Modes of vortex shedding and the wake pattern, case 3

Fig. 18 Pressure distribution on the foil at $t = 0$, $2T/8$, $4T/8$, and $6T/8$ for $S_h = 0.25$, 1, and 2

In case 1, for $S_h > 1$ (Fig. 12(a)), the maximum effective angle of attack occurs at midheaving locations ($t = 2T/8$ and $t = 6T/8$) as for the sinusoidal case. However, this angle is larger than in sinusoidal case, which leads to an increase of the lift and thrust magnitude at the middle of each half cycle as shown in Fig. 13. On the other hand, for $S_h < 1$, the effective angle of attack is maximal in areas close up to minimum ($t = 4T/8$) and maximum heaving locations ($t = 0$ and $t = T$). This considerably affects the time of leading edge vortex formation and shedding that impact the forces amplitude and position during the flapping cycle.

In case 2 (Fig. 12(b)), it can be seen that the nonsinusoidal pitching trajectory has a negligible effect on the effective angle of attack profile compared to that of nonsinusoidal heaving trajectory. For case where $S_\theta > 1$, the effective angle of attack profile remains similar to that of sinusoidal trajectory. As a result, the thrust force generated in this case remains comparable to that of sinusoidal trajectory. For the case $S_\theta < 1$, the effective angle of attack presents a double maximum close to midheaving positions. Therefore, a little increase is observed in the thrust force compared to that of sinusoidal trajectory.

In case 3 (Fig. 12(c)), the effective angle of attack profile is similar to case 1. It is concluded that the effective angle of attack is dominated by the nature of the heaving motion while the nature of the pitching motion has a negligible effect.

To better understand how the motion trajectory affects the flapping airfoil propulsive performances, quantitative comparisons of the instantaneous aerodynamic coefficients (C_D and C_L) are carried out together with qualitative comparisons using wake structure visualizations behind the flapping airfoil.

3.2.1 Effect on the Aerodynamic Coefficients. The nonsinusoidal heaving and pitching motions modified deeply the flow structure and the vortex shedding process behind the flapping

airfoil. This substantially impacts the drag (C_D) and lift (C_L) coefficients. Figure 13 shows the temporal variation of C_D and C_L over one flapping cycle. A remarkable behavior of the drag and lift coefficients is observed when compared to the reference case (sinusoidal trajectory) where C_D and C_L adopt a pseudo-sinusoidal shape. In all cases, the mean drag coefficient is negative, indicative of thrust production. Moreover, high values of negative drag coefficient are obtained using nonsinusoidal trajectories corresponding to the flattening parameters different to 1 (S_h greater than 1 and S_θ less than 1). The peak of thrust forces (negative drag) observed in Fig. 13 are associated with the peak of the effective angle of attack and the vortices created at the leading edge. Higher lift coefficients are registered for nonsinusoidal trajectories realized with $S_h = 0.25$ and/or $S_\theta = 0.25$ due to the vortex shedding mode 2P characterizing these cases.

3.2.2 Effect on the Vortex Shedding Process. Flow visualization around the flapping airfoil shows that the vortex shedding process is greatly affected by nonsinusoidal trajectories. In fact, the wake rearranges in new configurations different to that of the sinusoidal case. The symbols S and P introduced by Williamson and Roshko [40] to classify the vortex shedding modes are adopted: "S" stands for a single vortex and "P" for a pair of vortices of opposite signs.

3.2.2.1 Reference case (sinusoidal flapping motion). The 2S mode (Fig. 14) is observed in the reference sinusoidal flapping motion case ($S_h = S_\theta = 1$). In this mode, two vortices are shed per cycle. The first one, shed in the upstroke phase, is rotating clockwise while the second one, produced during the downstroke phase, is rotating counter-clockwise. These paired and rearranged vortices travel along the wake centerline to form the well-known von Karman eddy street but in its propulsive configuration. The interaction between these vortices produces a jet-like flow
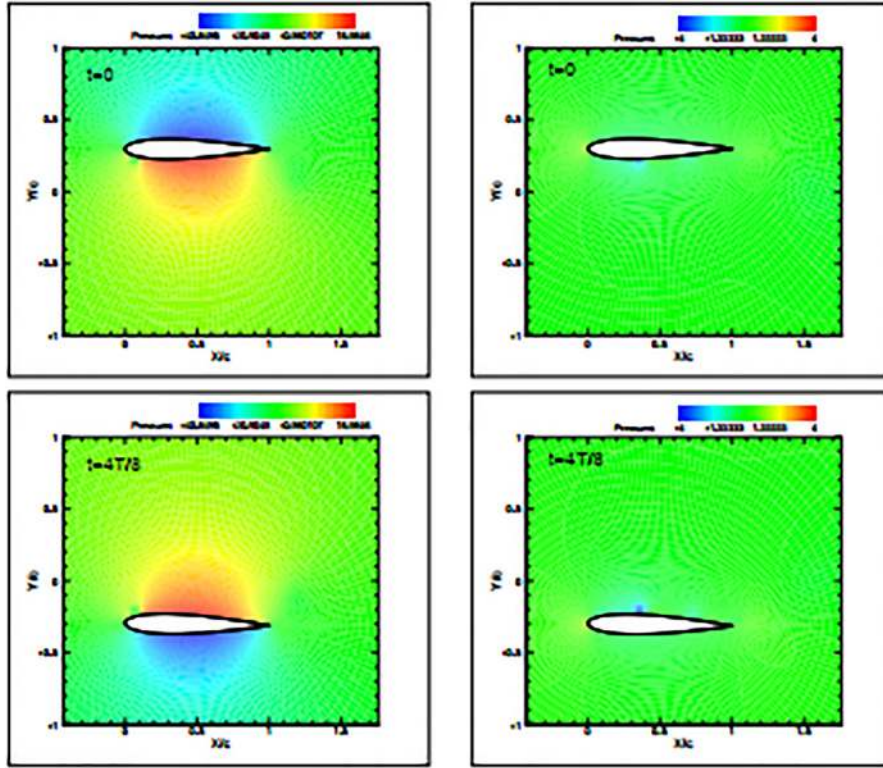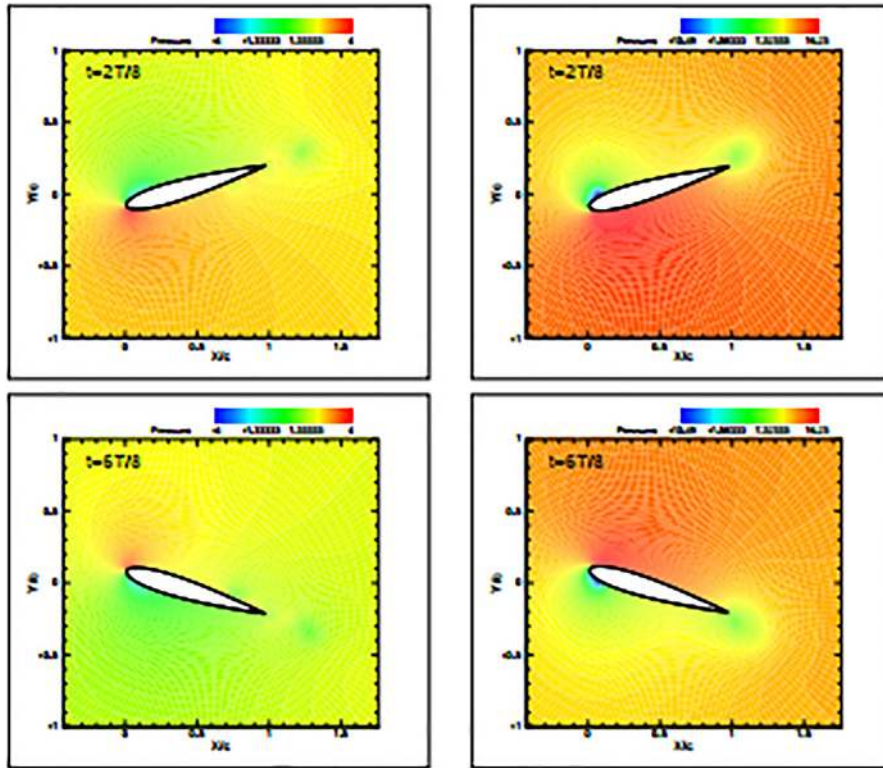
Fig. 19 Pressure distribution: (a) at $t = 0$ and $t = 4T/8$ for $S_h = 0.25$ (left) and $S_h = 1$ (right) and **(b)** at $t = 2t/8$ and $t = 6T/8$ for $S_h = 1$ (left) and $S_h = 2$ (right)

directed in downstream direction. By opposite reaction, this flow generates a thrust force directed upstream. It is observed that the 2S mode is associated with the case of the best propulsive efficiency.

3.2.2.2 Case of nonsinusoidal flapping motion. A combination of sinusoidal and nonsinusoidal flapping motions results in new wake configurations (2S, 2P, 2P_0) as shown in Figs. 15, 16, and 17.
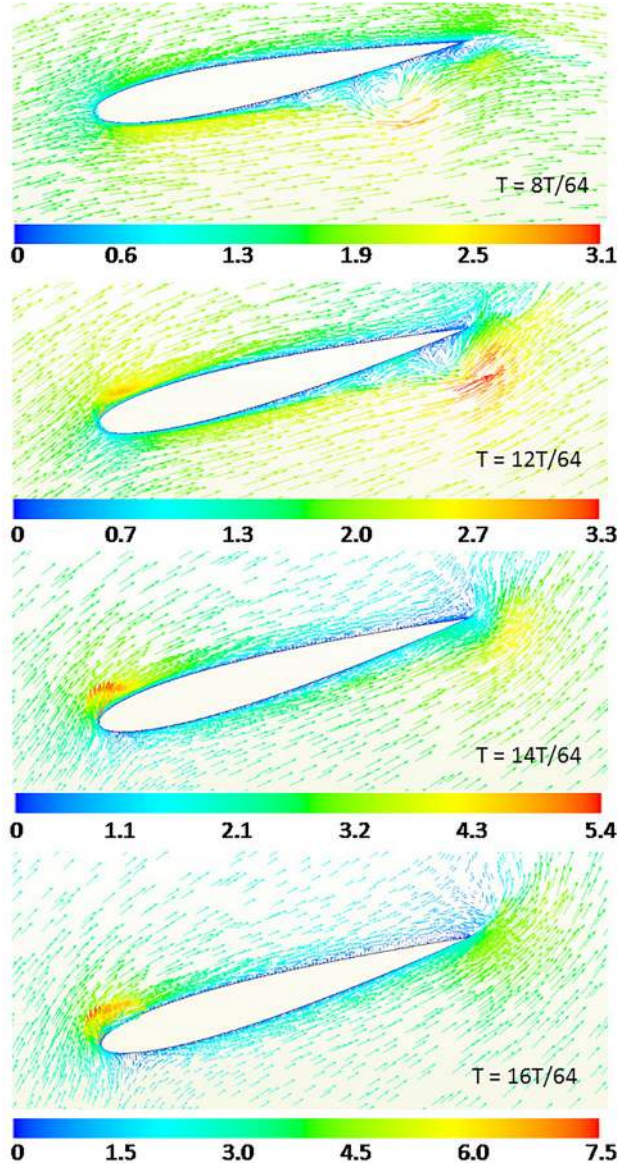
Fig. 20   Relative velocity for $S_h = 2$

- The $2P$ vortex shedding mode: This mode appeared for: $S_h < 1$, $S_\theta > 1$, and S_h and $S_\theta < 1$. Two counter-rotating vortices are shed in each half-cycle. The first vortex forms on the leading edge and the second on the trailing edge releasing thus two vortices pairs per cycle. For $2P$ mode, the vortex shedding frequency remains equal to that of the $2S$ mode [41] but causes a large increase in the lifting force relatively to that for the sinusoidal trajectory. This can be explained by the intensity of the vortex formed at the leading edge.
- The $2P_0$ vortex shedding mode appears for both $S_h > 1$ and S_h and $S_\theta > 1$ cases. This mode is a transition between $2P$ and $2S$ in such a way that two counter-rotating vortices are shed from the airfoil each half cycle as in the $2P$ mode. However, in $2P_0$ mode, the first vortex is largely more intense than the next shedded one, which is much weaker and disappears rapidly in the wake. For this mode, the far wake is similar to that of the $2S$, with the difference that the developed forces by the vortices are significantly different. In this study, the best propulsive force is obtained with $2P_0$ mode.
- The $2S$ vortex shedding mode: This mode is appeared for $S_\theta < 1$. In this case, the wake configuration is similar to that of sinusoidal trajectory, with the difference that the vortices

intensity is slightly higher. Therefore, the thrust produced is higher to that of the sinusoidal case.

4   Discussion

The objective of this section is to discuss the reasons for the effects of nonsinusoidal motion trajectories on the propulsive performance, i.e., the physics behind the changes of lift and propulsion forces reported previously. The attention is focused here on three cases: $S_h = 1$, 0.25, and 2, with a constant $S_\theta = 1$. Indeed, a major change in the thrust and lift forces has been observed in Sec. 3.2, for nonsinusoidal heaving motions, while the modification of the pitching motion was found to have only a slight influence on the forces. An increase of the mean thrust force of about 110% was obtained for $S_h = 2$. Conversely, at low value of S_h, a significant but smaller increase of the propulsion force was observed. In both cases though, the propulsive efficiency was significantly decreased, compared with the reference case $S_h = 1$. These effects of the flapping trajectory on the mean aerodynamic forces are related to major changes in the time evolutions of the drag and lift coefficient, depending on the value of S_h, which in turn are related to the changes observed in the instantaneous angles of attack. Another consequence on the nonsinusoidal heaving motion is the switch of the vortex shedding pattern from $2S$ to $2P$ and $2P_0$ modes, for $S_h = 0.25$ and $S_h = 2$, respectively.

The large increase of the mean propulsive force for $S_h = 2$ is mainly related to the two peaks of negative drag coefficients obtained just before $t = T/4$ and $3T/4$ (see Fig. 13), which are not present for $S_h = 1$ or lower values. As for $S_h = 0.25$, the two moderate peaks of negative drag observed at $t = 0$ and $T/2$ are partially counterbalanced by a larger positive draft in between, which eventually leads to the small increase of mean propulsive force mentioned previously. In that case, the two peaks at $t = 0$ and $T/2$ come with a major increase of the lift coefficient at the same time. Figure 18 shows the differences of pressure distribution on the foil surface at $t = 0$, $2T/8$, $4T/8$, and $6T/8$, which are thus the four time slots where large modifications of lift and/or drag are observed for $S_h = 2$ and/or $S_h = 0.25$: the increase of the foil load, compared with the reference case $S_h = 1$, can be clearly seen at the different times indicated hereinabove.

However, these large modifications of the pressure field result in very different effects on the thrust and lift forces, depending on the value of S_h. Indeed, for $S_h = 0.25$, the massive increase of the foil load occurs at zero pitching angle, at two times where the foil is decelerating the heaving motion up ($t = 0$) or down ($t = T/2$). The effect is symmetrical and opposite: in the upward position, a positive lift is obtained, while in the downward position, the exact same negative lift is obtained (Fig. 19(a)). So, the cumulative effect on the mean lift coefficient is zero. Conversely, the load increase for $S_h = 2$ is observed at mid-distance from the top and bottom positions, when the foil has the maximum pitching angle. Consequently, even if the suction and pressure sides are reversed in the upward and downward motions, the instantaneous pressure integration results both time in a negative force, i.e., a contribution to the foil propulsion (Fig. 19(b)). It explains the final significant increase of the thrust mean force.

The large increase of the foil load for $S_h = 2$, at $t = 2T/8$ and $6T/8$, is made possible by the absence of major flow separation and recirculation on the foil walls. As can be seen in Fig. 20, the vortex on the bottom wall, which was resulting from the final heaving deceleration at the end of the previous period, is evacuated downstream just before the maximum pitching angle. The detachment of the vortex from the foil trailing edge brutally changes the circulation around the profile, and subsequently raises the pressure levels on the foil (see Fig. 21). This mechanism is combined with the large increase of the pressure gradient at the leading edge on the foil upper side, due to the increase of the pitching angle, and eventually provides the maximum loading at $t = 16T/64$.

This favorable flow configuration is the result of the differences of heaving trajectories. Figure 22 shows the position of the foil as a
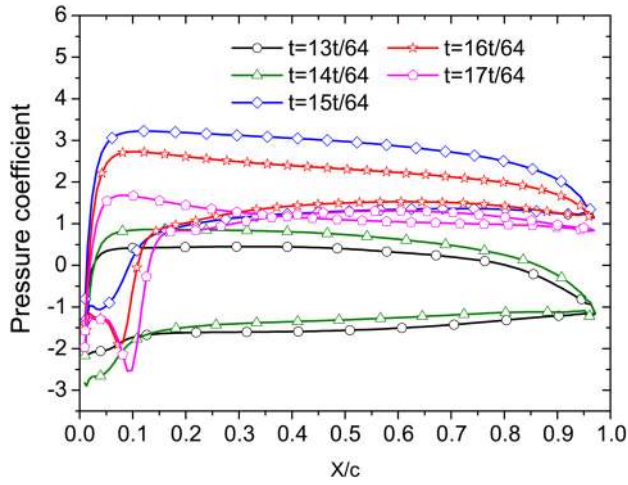
Fig. 21 Evolution of the foil load between *t* = 13*T*/64 and 17*T*/64, for *S_h* = 2

function of the vertical motion, for the three values of S_h considered here. The primary information is that the maximum pitching angle corresponds to the maximum heaving speed for $S_h = 1$ and $S_h = 2$, while it occurs at minimum heaving speed for $S_h = 0.25$ (see Fig. 23). In addition, the foil is vertically decelerating in the latter case between $t = T/8$ and $2T/8$, while it is accelerating in the other cases. More specifically, for $S_h = 2$ the time $t = 2T/8$ corresponds to the maximum amplitude of acceleration. These differences in the heaving trajectory directly result in the different pressure loads obtained at $t = 2T/8$. Specifically, the largest speed of heaving motion, combined with the acceleration unsteady terms, provides a much higher foil load for $S_h = 2$, compared with $S_h = 1$. The analysis of the different heaving trajectories also explains the brief major increase of the foil load at $t = 0$ and $t = T/2$, for $S_h = 0.25$: indeed, the deceleration/acceleration is maximum just before and after these instants, which generates a massive increase of the pressure difference between both sides of the foil.

It can be noticed for $S_h = 0.25$ that the heaving large decelerations/accelerations immediately before and after $t = 0$ and $t = T/2$ also have a positive effect on the thrust force, although it is moderate, compared with the case $S_h = 2$. Indeed, two significant negative peaks of thrust coefficient are observed in Fig. 13, just before and after $t = 0$ and $t = T/2$. It means that a small pitching angle is

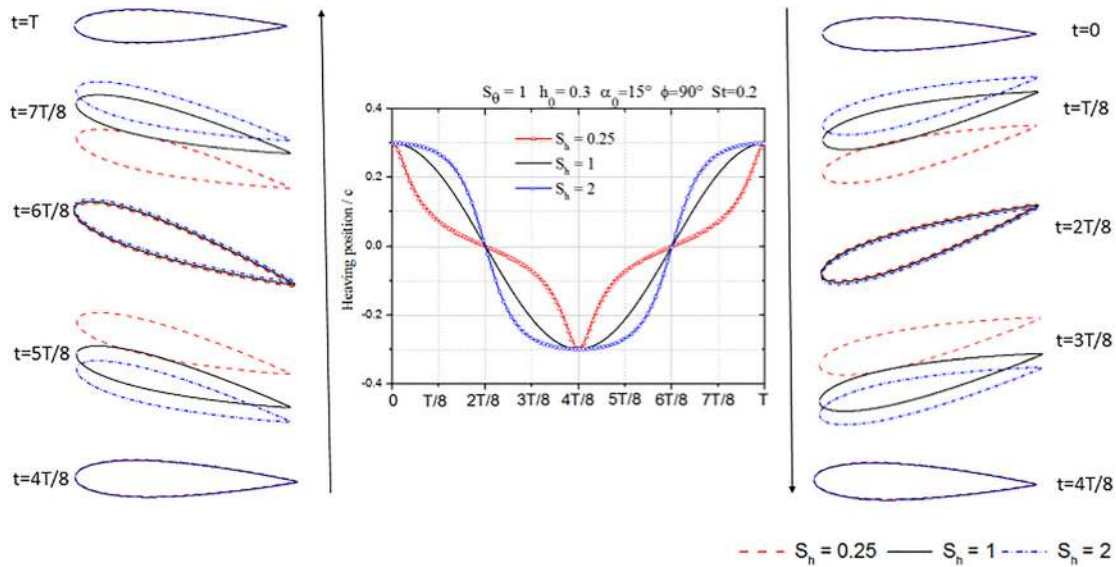**Fig. 22 Position and orientation of the foil during one flapping cycle for *S_h* = 0.25, *S_h* = 1 and *S_h* = 2**
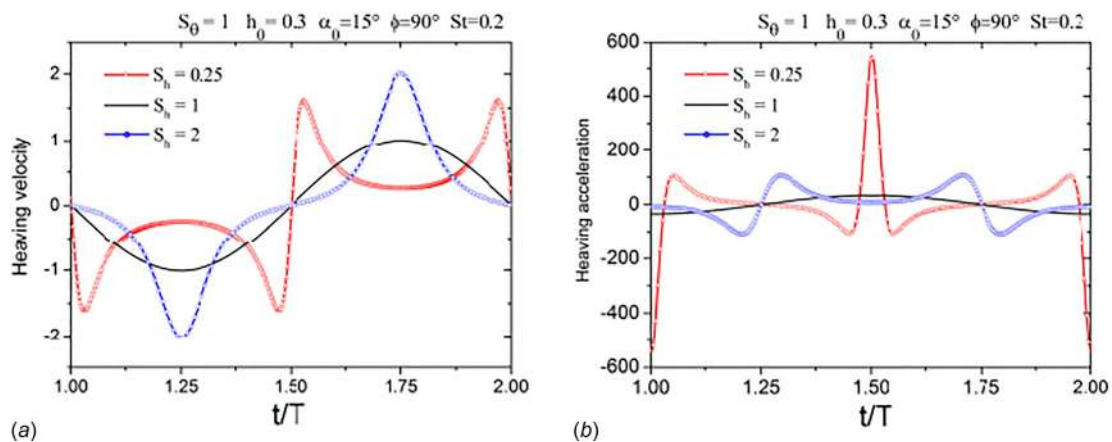

Fig. 23 (*a*) velocity and (*b*) acceleration of the foil during one flapping cycle for *S_h* = 0.25, *S_h* = 1 and *S_h* = 2
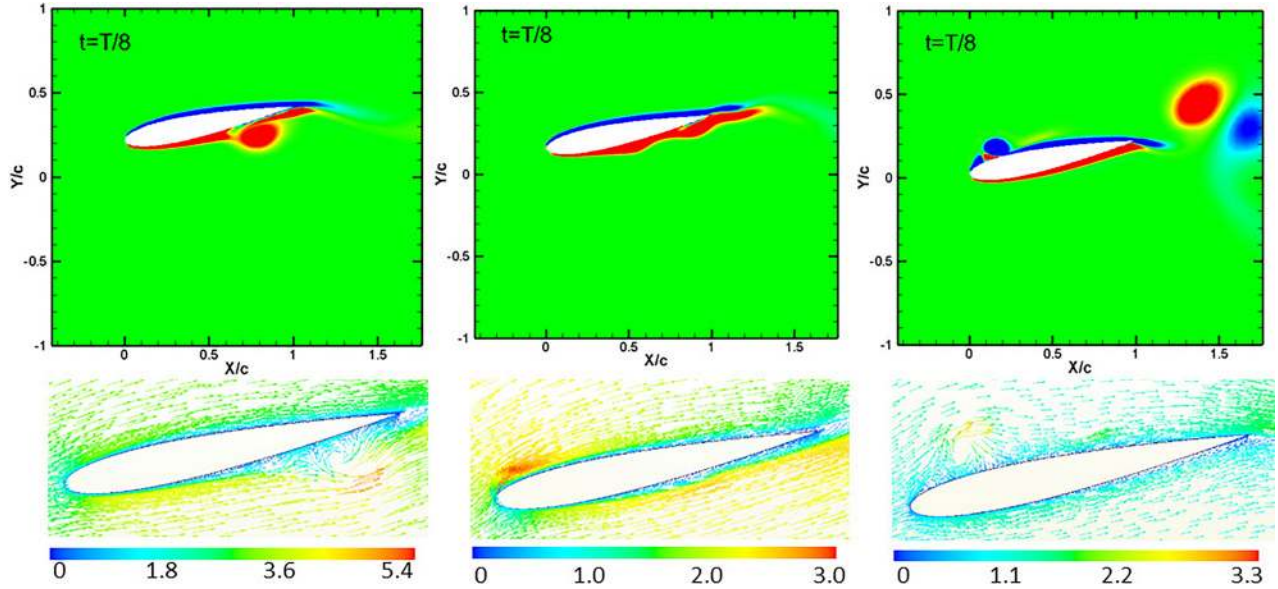
Fig. 24 Flow vorticity and relative velocity fields at $t = T/8$ for $S_h = 0.25$ (left), $S_h = 1$ (middle) and $S_h = 2$ (right)
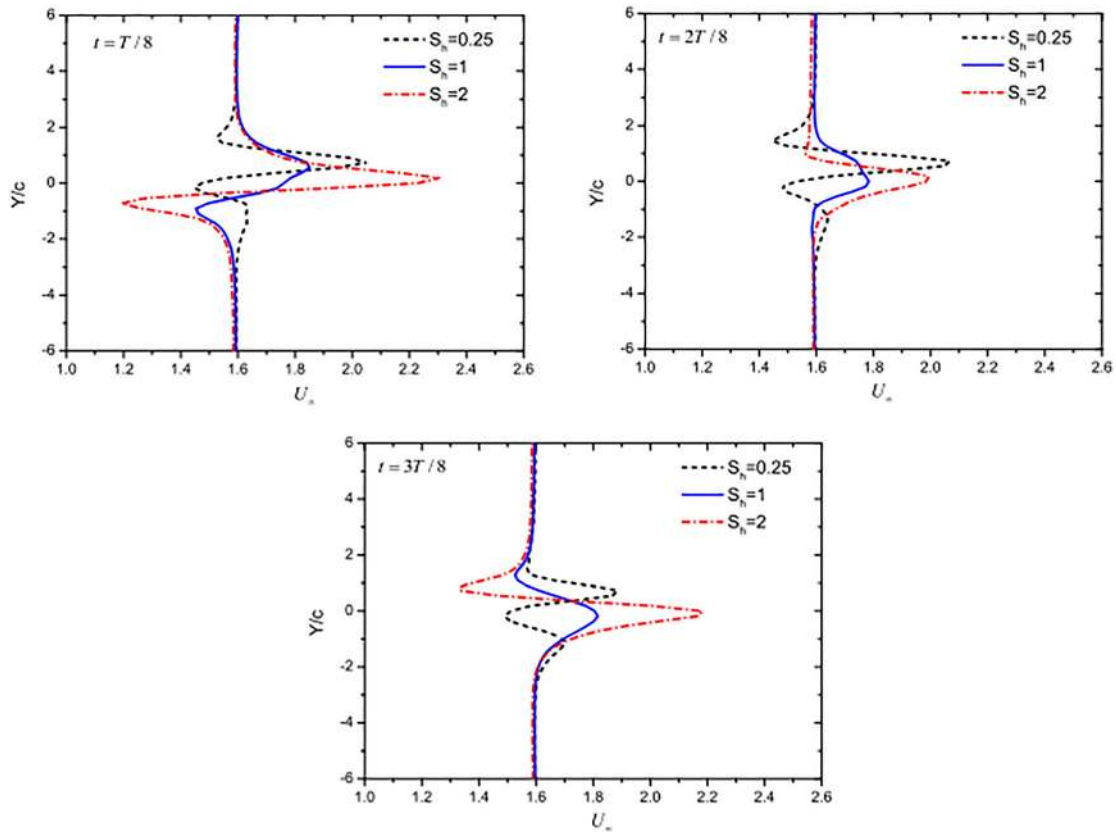

Fig. 25 Velocity profile in the wake of the foil at $t = t/8$, $2T/8$, and $3T/8$

sufficient to generate a significant force component in the horizontal direction, as the foil is highly loaded. The "hole" of thrust at the exact times $t = 0$ and $t = T/2$ is due to the decrease of that component when the foil passes the exact zero angle position. This result suggests that any transient acceleration of the heaving motion, with a higher amplitude than in the sinusoidal trajectory, will result in a significant increase of the propulsive force. This effect can be maximized by combining the maximum acceleration with the maximum pitching angle, as for $S_h = 2$.

The analysis of the flow vorticity from $t = 0$ to $t/4$ enables to understand why the major increase of the thrust force in the case $S_h = 2$ does not go with a propulsive efficiency as good as in the case $S_h = 1$. The increase of the input power coefficient observed in Fig. 11 for $S_h = 2$ and $S_h = 0.25$, compared with $S_h = 1$, can be attributed to the losses related to the flow recirculation and vortex sheddings observed in these two cases, on the upper and lower sides, respectively (see Fig. 24). For $S_h = 0.25$, the vortex on the suction side is generated by the fast heaving acceleration

experienced at the early stage of the motion, combined with the foil pitching motion. For $S_h = 2$, the vortex on the pressure side results from the end of the previous period, as the foil pitching angle decreases while the foil rapidly decelerates its vertical motion. The resulting deceleration of the boundary layer results in a flow separation and vortex generation. Such behavior is not observed for $S_h = 1$, where the vortices are generated at the foil trailing edge only, which minimizes the losses.

The wake observed in Sec. 3.2 in the three cases ($2S$, $2P$, and $2P_0$ flow patterns for $S_h = 1$, 0.25, and 2, respectively) is directly related to that: while the reverse von Karman vortex street is obtained for the sinusoidal foil motion, the additional vortices generated at the leading edge, due to the flow conditions mentioned hereinabove, result in the more complex $2P$ and $2P_0$ wakes. The velocity profiles in the wake of the foil, shown in Fig. 25 at three successive times, confirm the previous analysis: only a positive additional x component of velocity is found for $S_h = 1$, which is the signature of the propulsive force. For $S_h = 2$, this additional component is much higher, as expected, but the trade-off for that is a significant negative component in the outer region of the wake, due to the losses induced by the vortex shedding. This is also true, to some extent, for $S_h = 0.25$, but the improvement of the thrust force is much lower in that case, as seen previously.

5 Conclusions

In this study, the effects of motion trajectory on the propulsive performances and the shedding process of a flapping airfoil are examined. The flow structures and the forces acting on NACA0012 airfoil undergoing sinusoidal and nonsinusoidal heaving and pitching motions are investigated using the finite volume code STAR CCM+. The results obtained in the validation step show the ability of our numerical simulation to reproduce the main flow features obtained in previous experiments. It is established that the trajectory motion has a significant effect on the performances and the vortex-shedding mode of the flapping airfoil. The best propulsive efficiency is always obtained by the sinusoidal flapping trajectory. However, the use of nonsinusoidal flapping trajectory is found to improve considerably the thrust force generated by the flapping motion, especially for heaving motions with a flattening parameter higher than 1. Qualitatively, it is observed that the vortex-shedding mode shifts from $2S$ a sinusoidal trajectory to other configurations ($2S$, $2P$, $2P_0$) for nonsinusoidal trajectories.

The increase of the thrust force observed for nonsinusoidal heaving motions was discussed in more details by analyzing the flow field evolution. For $S_h > 1$, where the maximum thrust force is obtained, it was found that it is mainly due to the simultaneous maximum pitching angle and maximum acceleration of the heaving motion: this configuration provides the maximum force in the propulsion direction, resulting from the foil load. For $S_h < 1$, the large acceleration/deceleration at zero pitching angle also provides a significant increase of the propulsion force, compared with $S_h = 1$. So, it turns out that the main interest of nonsinusoidal heaving trajectory is a larger transient acceleration, which increases the foil load in all cases. The tradeoff for that increased force is an increase of the drag due to additional vortices generated at the foil leading edge, which eventually makes the drop of the propulsive efficiency.

Acknowledgment

Nomenclature

A = foil area, m^2
c = foil chord length, m
C_D = drag coefficient
C_L = lift coefficient
C_Z = moment coefficient
$\bar{C}_p$ = mean power coefficient
$\bar{C}_t$ = mean thrust coefficient
d = airfoil trailing edge displacement in vertical motion, m
f = flapping frequency, Hz
F_x = drag force, N
F_y = lift force, N
h_0 = nondimensional heaving amplitude
$h(t)$ = heaving motion
M_z = moment, N·m
p = pressure, Pa
Re = Reynolds number based on the chord length
  (Re $= \rho c U_\infty / \mu$)
S_h = flattening parameter of the heaving trajectory
S_θ = flattening parameter of the pitching trajectory
St = Strouhal number (St $= 2ch_0 f/U_\infty$)
St$_{TE}$ = Strouhal number is based on the trailing edge excursion
  (St$_{TE} = 2df/U_\infty$)
t = time, s
T = flapping period ($T = 1/f$), Hz
u = velocity component in x direction, m/s
U_∞ = freestream velocity, m/s
v = velocity component in y direction, m/s
X_P = chordwise position of pitching axis, m
y^+ = dimensionless wall distance
α_0 = effective angle of attack, deg
η = propulsive efficiency
$\theta(t)$ = pitching motion
θ_0 = pitching amplitude, deg
μ = dynamic viscosity, Pa·s
ν = kinematic viscosity ($\nu = \mu/\rho$), m^2/s
ρ = fluid density, kg m^{-3}
ϕ = phase angle between heaving and pitching motions, deg
ω = angular frequency ($\omega = 2\pi f$), rad/s

References

[1] Knoller, R., 1909, *Die Gesetze Des Luftwiderstands*, Verlag Des Sterreichischer Flugtechnischen Vereines, Wien, Austria.
[2] Betz, A., 1912, "Zeitschrift Faur Flugtechnik Und Motorluftschiffahrt," Beitrag Zur Erklarung Des Segelfluges, **3**, pp. 269–272.
[3] Katzmayr, R., 1922, "Effect of Periodic Changes of Angle of Attack on Behaviour of Airfoils," National Advisory Committee for Aeronautics, Washington, DC, Report No. NACA-147.
[4] Durand, W. F., 1935, *Aerodynamic Theory: General Aerodynamic Theory: Perfect Fluids[by] Th. von Kármán; J. M. Burgers*, Springer, Berlin.
[5] Jones, K. D., Dohring, C. M., and Platzer, M. F., 1998, "Experimental and Computational Investigation of the Knoller-Betz Effect," AIAA J., **36**(7), pp. 1240–1246.
[6] Theodorsen, T., 1949, "General Theory of Aerodynamic Instability and the Mechanism of Flutter," National Advisory Committee for Aeronautics, Langley Aeronautical Laboratory, Langley Field, VA, NASA Report No. NACA-TR-496.
[7] Garrick, I. E., 1937, "Propulsion of a Flapping and Oscillating Airfoil," National Advisory Committee for Aeronautics, Langley Aeronautical Laboratory, Langley Field, VA, NACA Report No. NACA-TR-567.
[8] Triantafyllou, G. S., Triantafyllou, M. S., and Grosenbaugh, M. A., 1993, "Optimal Thrust Development in Oscillating Foils With Application to Fish Propulsion," J. Fluids Struct., **7**(2), pp. 205–224.
[9] Anderson, J. M., Steritlien, K., Barrett, D. S., and Triantafyllou, M. S., 1998, "Oscillating Foils of High Propulsive Efficiency," J. Fluid Mech., **360**, pp. 41–72.
[10] Lai, J. C. S., and Platzer, M. F., 1999, "Jet Characteristics of a Plunging Airfoil," AIAA J., **37**(12), pp. 1529–1537.
[11] Triantafyllou, M., Techet, A. H., and Hover, F. S., 2004, "Review of Experimental Work in Biomimetic Foils," IEEE J. Oceanic Eng., **29**(3), pp. 585–594.
[12] Babu, M. N. P., Krishnankutty, P., and Mallikarjuna, J. M., 2014, "Experimental Study of Flapping Foil Propulsion System for Ships and Underwater Vehicles and Piv Study of Caudal Fin Propulsors," IEEE/OES Autonomous Underwater Vehicles (AUV), Oxford, MS, Oct. 6–9, pp. 1–7.
[13] Lee, T., and Su, Y., 2015, "Surface Pressures Developed on an Airfoil Undergoing Heaving and Pitching Motion," ASME J. Fluids Eng., **137**(5), p. 051105.
[14] Nguyen, T. A., Phan, H. V., Au, T. K. L., and Park, H. C., 2016, "Experimental Study on Thrust and Power of Flapping-Wing System Based on Rack-Pinion Mechanism," Bioinspiration Biomimetics, **11**(4), p. 046001.
[15] Siala, F., Totpal, A., and Liburdy, J., 2016, "Characterization of Vortex Dynamics in the Near Wake of an Oscillating Flexible Foil," ASME J. Fluids Eng., **138**(10), p. 101202.

[16] Tuncer, I. H., and Platzer, M. F., 1996, "Thrust Generation Due to Airfoil Flapping," AIAA J., **34**(2), pp. 324–331.

[17] Shyy, W., Berg, M., and Ljungqvist, D., 1999, "Flapping and Flexible Wings for Biological and Micro Air Vehicles," Prog. Aerosp. Sci., **35**(5), pp. 455–505.

[18] Young, J., and Lai, J., 2004, "Oscillation Frequency and Amplitude Effects on the Wake of Plunging Airfoil," AIAA J., **42**(10), pp. 2042–2052.

[19] Young, J., and Lai, J. C. S., 2007, "Mechanisms Influencing the Efficiency of Oscillating Airfoil Propulsion," AIAA J., **45**(7), pp. 1695–1702.

[20] Ashraf, M. A., Young, J., Lai, J. C. S., and Platzer, M. F., 2011, "Numerical Analysis of an Oscillating-Wing Wind and Hydropower Generator," AIAA J., **49**(7), pp. 1374–1386.

[21] Benkherouf, T., Mekadem, M., Oualli, H., Hanchi, S., Keirsbulck, L., and Labraga, L., 2011, "Efficiency of an Auto-Propelled Flapping Airfoil," J. Fluids Struct., **27**(4), pp. 552–566.

[22] Olivier, M., and Dumas, G., 2016, "Effects of Mass and Chordwise Flexibility on 2D Self-Propelled Flapping Wings," J. Fluids Struct., **64**, pp. 46–66.

[23] Chao, L. M., Cao, Y. H., and Pan, G., 2017, "A Review of Underwater Bio-Mimetic Propulsion: Cruise and Fast-Start," Fluid Dyn. Res., **49**(4), p. 044501.

[24] Ashraf, M. A., Young, J., and Lai, J. C. S., 2011, "Reynolds Number, Thickness and Camber Effects on Flapping Airfoil Propulsion," J. Fluids Struct., **27**(2), pp. 145–160.

[25] Deng, S., and Xiao, T., 2016, "Effect of Flexion on the Propulsive Performance of a Flexible Flapping Wing," Proc. Inst. Mech. Eng., Part G, **230**(12), pp. 2265–2273.

[26] Koochesfahani, M., 1989, "Vortical Patterns in the Wake of an Oscillating Airfoil," AIAA J., **27**(9), pp. 1200–1205.

[27] Read, D. A., Hover, F. S., and Triantafyllou, M. S., 2003, "Forces on Oscillating Foils for Propulsion and Maneuvering," J. Fluids Struct., **17**(1), pp. 163–183.

[28] Hover, F., Haugsdal, O., and Triantafyllou, M., 2004, "Effect of Angle of Attack Profiles in Flapping Foil Propulsion," J. Fluids Struct., **19**(1), pp. 37–47.

[29] Sarkar, S., and Venkatraman, K., 2005, "Numerical Simulation of Incompressible Viscous Flow Past a Heaving Airfoil," Int. J. Numer. Methods Fluids, **51**(1), pp. 1–29.

[30] Kaya, M., and Tuncer, I. H., 2007, "Path Optimization of Flapping Airfoils Based on NURBS," Parallel Computational Fluid Dynamics, Busan, South Korea, May 15–18, pp. 285–292.

[31] Kaya, M., and Tuncer, I. H., 2009, "Non-Sinusoidal Path Optimization of Dual Airfoils Flapping in a Biplane Configuration," *Parallel Computational Fluid Dynamics 2007*, Vol. 67, Springer, Berlin, pp. 59–66.

[32] Xiao, Q., and Liao, W., 2009, "Numerical Study of Asymmetric Effect on a Pitching Foil," Int. J. Mod. Phys. C, **20**(10), pp. 1663–1680.

[33] Xiao, Q., and Liao, W., 2010, "Numerical Investigation of Angle of Attack Profile on Propulsion Performance of an Oscillating Foil," Comput. Fluids, **39**(8), pp. 1366–1380.

[34] Lu, K., Xie, Y. H., and Zhang, D., 2013, "Numerical Study of Large Amplitude, Nonsinusoidal Motion and Camber Effects on Pitching Airfoil Propulsion," J. Fluids Struct., **36**, pp. 184–194.

[35] Esfahani, J. A., Barati, E., and Karbasian, H. R., 2015, "Fluid Structures of Flapping Airfoil With Elliptical Motion Trajectory," Comput. Fluids, **108**, pp. 142–155.

[36] Yang, S., Liu, C., and Wu, J., 2017, "Effect of Motion Trajectory on the Aerodynamic Performance of a Flapping Airfoil," J. Fluids Struct., **75**, pp. 213–232.

[37] Kinsey, T., and Dumas, G., 2012, "Optimal Tandem Configuration for Oscillating-Foils Hydrokinetic Turbine," ASME J. Fluids Eng., **134**(3), p. 031103.

[38] Siemens, 2016, "STAR-CCM+® Documentation Version 11.06," Siemens PLM Software, accessed Jan. 15, 2017, http://www.cd-adapco.com/products/star-ccm

[39] Boudis, A., Benzaoui, A., Oualli, H., Guerri, O., Bayeul-Laine, A. C., and Delgosha, O. C., 2018, "Energy Extraction Performance Improvement of a Flapping Foil by the Use of Combined Foil," J. Appl. Fluid Mech., **11**(6), pp. 1651–1663.

[40] Williamson, C. H. K., and Roshko, A., 1988, "Vortex Formation in the Wake of an Oscillating Cylinder," J. Fluids Struct., **2**(4), pp. 355–381.

[41] Govardhan, R., and Williamson, C. H. K., 2000, "Modes of Vortex Formation and Frequency Response of a Freely Vibrating Cylinder," J. Fluid Mech., **420**, pp. 85–130.